**FINAL REPORT**

On: **IDENTIFICATION AND CONTROL OF GRAVITY RELATED DEFECT FORMATION DURING MELT GROWTH OF ELECTRO-OPTIC SINGLE CRYSTALS BISMUTH SILICATE ($Bi_{12}SiO_{20}$).**

Grant No.: NAG8-1487 (3)

Period: Feb. 01-1998 – Dec.31-2003

Submitted to: 000410:NASA-Marshals Space Flight Center (LU)
Frazier, Joan
George C. Marshall Space Flight Center
Marshall Space Flight Center, AL 35812
Mail Code MG 21

Project Originator: August F. Witt

Submitted by: Wuensch, Bernhardt J. (PI)
Department of Materials Science and Engineering
And Materials Processing Center
Massachusetts Institute of Technology
Cambridge, MA 02139

Prepared by: Becla, Piotr and Wiegel, Michaela E.K.* (Co-Inv.)
Department of Materials Science and Engineering
Massachusetts Institute of Technology
Cambridge, MA 02139 and
* MIT Lincoln Laboratory

**May** 2004

## Summary

A research carried out under Award Number NAG8-1487 was aimed at to the design, conduct and analysis of experiments directed at the identification and control of gravitational effects on crystal growth, segregation and defect formation in the Sillenite system: bismuth silicate ($Bi_{12}SiO_{20}$). Correlation analyses was conducted in order to establish the influence of gravity related defects introduced during crystal growth on critical, application specific properties.

Achievement of the stated objectives was conducted during the period from Feb. 01, 1998 to Dec. 31, 2003 with the following anticipated milestones:

- Establishment of capabilities for (a) reproducible Czochralski and Bridgman-type growth of BSO single crystals and (b) for comprehensive analysis of crystalline and chemical defects as well as for selective property characterization of grown crystals (year 1).
- Design and execution of critical space growth experiment(s) based on analyses of prefatory space results (experiments aimed at establishing the viability of planned approaches and procedures) and on unresolved issues related to growth, segregation and defect formation associated with conventional growth in Bridgman geometries. Comparative analysis of growth under conventional and under μ-g conditions; identification of gravity related defect formation during conventional Bridgman growth and formulation of approaches for their control (years 2 and 3).
- Development of a charge confinement system which permits growth interface demarcation (in a μ-g environment) as well as minimization of confinement related stress and contamination during growth; design of complementary μ-g growth experiments aimed at quantitative μ-g growth and segregation analyses (year 4).
- Conduct of quantitative μ-g growth experiments directed at (a) identification and control of gravity related crystalline and chemical defect formation during single crystal growth of $Bi_{12}SiO_{20}$ and at (b) defect engineering - the development of approaches to the controlled generation during crystal growth of specified point defects in homogeneous distribution (year 5).

The proposed research places focus on a class of materials which have outstanding electrical and optical properties but have so far failed to reach their potential, primarily because of our inability to control adequately their stoichiometry and crystal defect formation as well as confinement related contamination and lattice stress.

## Background

Electro-optical properties of materials (1) provide the basis for a large variety of devices ranging from bulk modulators and wave guides to optical deflectors and holographic storage systems (2,3). The spectrum of electro-optical materials with properties which suggest their application in devices is large (4). It includes tetragonal bronzes, perovskites, ionic materials (the KDP family), semiconductors and a steadily increasing number of organic compounds. The number of different materials currently used in devices, however, is limited, being restricted to compounds, which can be produced in single crystal form at required

dimensions and with a degree of perfection at which critical application-specific properties exceed minimum requirements (5).

When comparing the status of device quality materials for electro-optical applications (6) with that for electronic applications, it is conspicuous that progress in production of electro-optical materials lags seriously behind. This deficiency is compounded by the fact that CVD- and MBE-based thin film technologies have steadily increasing, but as yet only limited, applicability in electro-optics (7); it therefore relies heavily on the availability of "bulk" material with a minimum of light loss due to scattering centers (defects) of varying origin and nature (8,9).

Fig.1 Optical scattering centers in commercial SBO (Current investigation)

Primary limitations in our ability to produce device quality electro-optical materials are at present imposed by excessive formation of crystalline and chemical defects during single crystal growth (10,11). Defects such as precipitates, gaseous inclusions, dislocations, low angle grain boundaries and lattice strain, among others, adversely affect critical properties and thus the performance of these materials in devices. Additional complications arise from difficulties in meeting the fundamental requirement of compositional uniformity on a microscale over macroscopic dimension, a requirement which applies to stoichiometry as well as to the incorporation of optically active minority constituents (dopants). In many instances the use of particular opto-electronic materials in devices is in fact precluded by excessive structural and chemical deficiencies.

Slow progress in efforts directed at efficiently meeting application-specific property requirements in electro-optical materials can largely be attributed to their stoichiometric and structural complexity, to the high melting points of oxides and to the corrosiveness of the molten state. It must in part also be attributed to inadequacies in monitoring and control of the growth process and related defect formation. Last but not least, existing problems relate also to fundamental limitations in our understanding of the processes associated with crystal growth and segregation under conditions other than "ideal".

The complexity of defects in electro-optical materials such as SBN, [$(Sr,Ba)Nb_2O_6$] (12) and BSO [$Bi_{12}SiO_{20}$] (13) has so far prevented the exact determination of their nature and origin

(2,5,11). There exists, however, strong experimental evidence (14) and theoretical grounds suggesting that their formation is in the main related directly or indirectly to complications related to heat transfer and to gravity induced convective interference with (a) the crystal growth process and (b) segregation (15). Efforts directed at controlling such convection-related defect formation during crystal growth, while successful in a multitude of semiconductor systems (16), have so far been largely ineffective in oxides such as SBN and BSO.

**Literature:**


1. Weber, H.-J, Crystals: Growth, Prop. and Appl., Springer 11,(1988)
2. Neurgaonkar, R.R., Optical Eng'g. 26, (1987) 392. Neurgaonkar, R.R., J. Opt. Soc. Am. 3, (1986) 274.
3. Kaminow, P. Appl. Phys. Lett. 24, (1974) 622. Chen, F.S., Proc. IEEE 58, (1970) 1440; Kaminow, P. and E.H. Turner, Appl. Optics, 5, (1966) 1612;
4. Günther, P., Phys. Rep. 93, (1982) 199. Papuchon, M. et al., Appl. Phys. Lett. 27, (1975) 289. Wemple S.H. et al., Appl. Solid State Sci. 3, (1972) 262. Weber, H.-J, Crystals, Growth, Prop. and Appl., Springer 11,(1988) 133.
5. Valley, G.C., et al., Ann. Rev. Mat. Sci. 18, (1988) 165.
6. Tanguay, A. Jr., Optical Eng'g. 24, (1985) 002.
7. Neyer, A., and W. Sohler, Appl. Phys. Lett. 35, (1979) 256
8. Schlaak, H.F., and R.Th. Kernsten, Opt. Comm. 36, (1981) 186.
9. Casasent, D., et al., Appl. Optics 20, (1981) 4215.
10. Oberschmid, R., Phys. Stat. Sol.(A), (1985) 263.
11. Krishnamurthy, D., J. Mat. Sci. Lett. 12, (1993) 1218. Just, D. et al Mat., Science and Eng'g. B9, (1991) 469.
12. Ballman, A.A. J. Cryst. Growth, 1, (1967) 37.
13. Ballman, A.A. J. Cryst. Growth, 1, (1967) 311.
14. Monchamp, R.R. J. Cryst. Growth 141, (1994) 178 Sobolev, A.T. et al. Kristallogrraphica, 23, (1978) 179 Miyazawa, S. J. Cryst. Growth, 49, (1980) 515
15. Carruthers, J.R., J.Cryst.Growth, 36, (1976) 212. Brandle, D., J. Cryst. Growth, 42, (1977) 400. Miller, D. J. Cryst. Growth 44, (1978) 121. Brice, J.C. et al. Philips Tech. Rev. 37, (1977) 250.
16. Utech, H.P., and M.C. Flemings, J. Appl. Phys. 37, (1966) 2021. Hurle, D.T.J. Proceedings, ICCG (1966); A.F. Witt et al. J. Mat. Sci. 5, (1970) 822.


## Motivation for Proposed Research

The growth related defects in oxide single crystals are found to be fundamentally similar to those in semiconductors. Primary differences relate to more complex stoichiometries and to increased sensitivity of critical, application-specific properties to defects. Thus the complex, interactive defect structures, which comprise crystallographic defects, inclusions, confinement related contamination, segregation and stress effects, observed, for example in SBN and BSO, adversely affect optical absorption and charge carrier mobility to a point

which renders these materials unsuitable for a multitude of device applications such as holographic data storage and parametric amplification, for example.

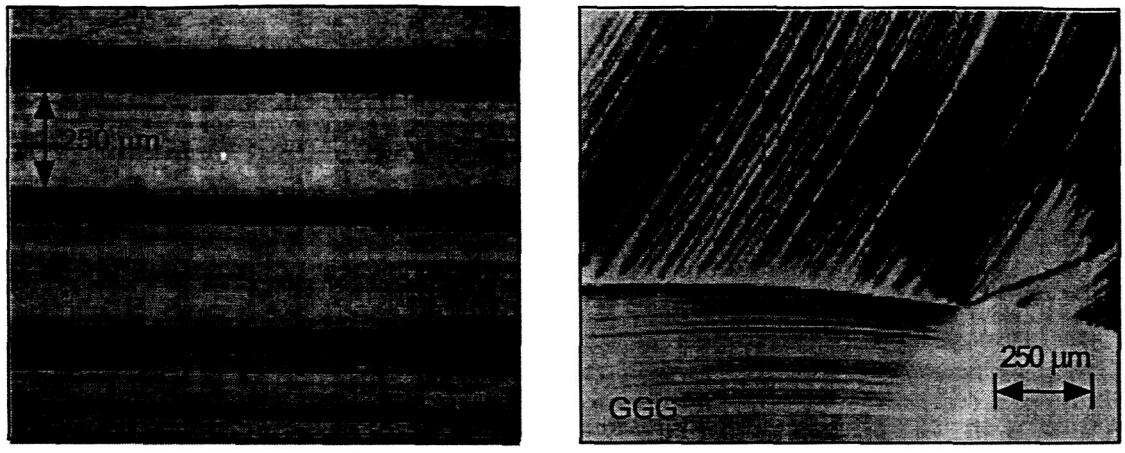


Fig. 2a Compositional striations in SBN [Monchamp, R (14)] and in GGG [Miller, D (15)]

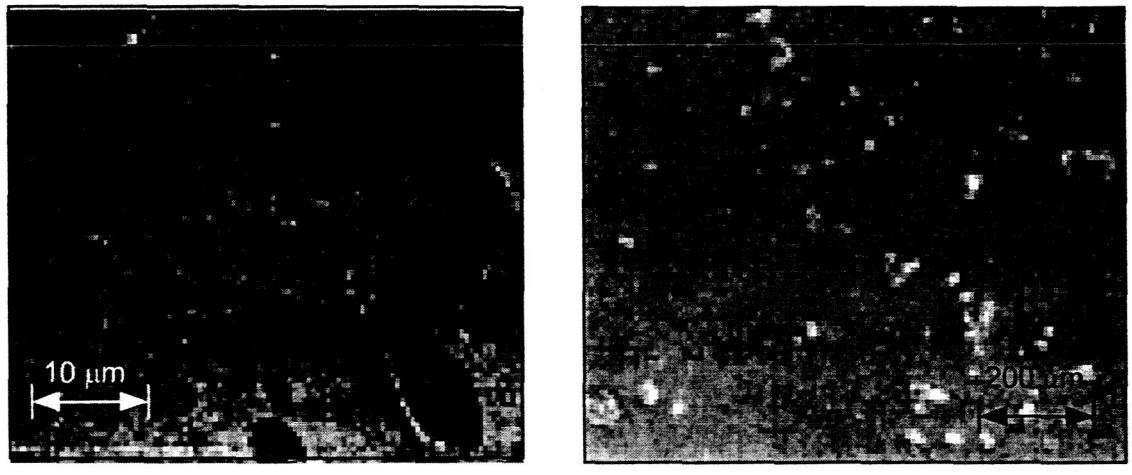


Fig. 2b Gaseous in crystalline inclusions in SBO [Krishnamurthy, D (11)]

**The rationale** for submission of this research project was reflected in the functional dependency of the primary driving forces for convection in growth systems, as formulated, for example, through the Rayleigh ($R_a$) number:

$$R_a \propto g.l^3.\Delta T$$

Accordingly, melt and solution growth experiments conducted in a microgravity environment ($g \sim 10^{-5}$ to $10^{-6}$) experience a reduction in the ($\Delta\rho$-related) driving force for convection by 5 to 6 orders of magnitude. The complexity and density of convection related defect structures (1,2) formed during growth are thus expected to be significantly decreased and critical, as yet unresolved, issues on growth and segregation should become amenable to more detailed analysis, a prereqisite in efforts to ultimately establish growth conditions under which defect formation is controllable.

It must be pointed out that melt and solution growth-systems in a micro gravity environment are not free of convective driving forces. Both temperature and concentration gradients on free melt surfaces, and to a minor extent on melt-solid interfaces, will result in gradients of surface tension and thus constitute driving forces for convective (bulk) melt flows (3) formulated through the Marangoni ($M_m$) number:

$$M_a \propto \delta\gamma/\delta T.\mathbf{l}.\Delta T$$

Extensive experimental evidence of surface tension driven convection has been reported for simulated ground-based growth geometries (4). Similarly some results from growth experiments in space have been interpreted as due to Marangoni-type convection (5). It is hoped that the presently proposed experiments provide a needed, expanded data base for verification and/or, as indicated, modification of the established theoretical models on convective heat and mass transport in melt growth of oxide systems (6)

**The primary issues of scientific and technological concern in this project was:**

- Elucidation of the origin and nature of periodic and random striations in oxide single crystals grown from the melt (3,4);
- Determination of the mode of formation and incorporation of precipitates and gaseous inclusions in oxides (5);
- Determination of the origin of stress-birefringence (6);
- Identification of the chemical and/or crystallographic nature of defects comprising the spectrum of "deep traps" in the band gap of oxides (7,8);
- Determination of the ($\Delta\rho$-related) convective contribution to heat transfer in the melt, and its effect on the growth process and the morphology of the crystal growth interface (9);
- Development of approaches to "virtually unconfined melt growth" under reduced gravity conditions (10);
- Consolidation of the existing data base for crystal growth in a micro-gravity environment.

The selective reduction of the primary driving force for convective melt flows, achieved in microgravity growth experiments, facilitate the establishment of cause and effect relationships for defect formation; it also advance our understanding of the crystal growth process and thus provide a basis for (a) enhanced property control during crystal growth (11-13) and (b) the conduct of effective defect engineering directed at the optimization of application-specific properties in electro-optical materials(6,14). (It should be pointed out that the outstanding optical properties of BSO are not "native" (15) but "induced" through the action of point defects which are as yet to be identified through defect engineering.

**Literature:**

1. Shepanov, S.I. et al. Sov. Phy. Tech. Phys. 29 (1984) 703; Lukasiewicz, T. et al. Kristall und Technik, 15 (1980) 267. Gevay, G. Progr. Cryst. Gr. Charact'n. 15 (1987) 145 Horowitz, A. et al. J. Cryst. Growth 78 (1986) 121 Bieler, Ch. et al. Nucl. Instr. Methods A234 (1985) 435 Smet, F. et al. J. Cryst. Growth 100 (1990) 417 Arzumanyan, G.A. J. Cryst. Growth 99 (1990) 859
2. Shepanov, S.I., et al. Sov. Phys. Tech. Phys. 29 (1984) 703.
3. Sobolev, A.T. et al. Kristallografiia, 23 (1978) 179 Monchamp, R.R. J. Crystal Growth 141 (1994) 178. Krishnamurthy, R. et al. J. Mats. Sci. Letters 12 (1993) 1220. Miller, D. J. Cryst. Growth 44 (1978) 121.
4. Wilcox, W.R. et al. J. Cryst. Growth 28 (1975) 8. Ostrach, S. et al. COSPAR Space Res. 19 (1979) 563.
5. Hurle, T.D.J. Cryst. Gr. and Matter (1977) 549 Ed. Kaldis, N. Holland Schwabe, D. J. Cryst. Growth 43 1978) 305.
6. Kölker, H. J. Cryst. Growth 50 (1980) 852. Eyer, A. et al. J. Cryst. Growth 71 (1985) 173.
7. Derby, J. J. et al. J. Cryst Growth 121 (1992) 473. Brown, R.A. et al., J. Cryst. Growth 96 (1989) 609.
8. Brice, J.C. and Whiffin, P.A.C. J. Crystal Growth 38 (1977) 245. Burton, T.M., et al. J. Crystal Growth 23 (1974) 21.
9. Kopylov, J.L., Proc. Ind. Acad. Sci. 57 (1991) 145 Ming, Nai-ben J. Cryst. Growth 99 (1990) 1309.
10. Lauer, R.B. et al. Appl. Phys. Let. 17 (1970) 15. Attard, A.E. et al. Applied Optics 25 (1986) 18. Efendiev, S.M.et al. Phys. Stat. Sol.(B), 162 (1990) 281. Oberschmid, R., Phys. Stat. Sol. (A), 89 (1985) 263.
11. Benjelloun, N., et al. J. Appl. Phys. 64 (1988) 4013. Refregier, Ph. et al. J. Appl. Phys., 58 (1985) 45. Jain, M.G. J. Appl. Phys. 64 (1988) 2022. Mullen, R.A. et al. J. Appl. Phys. 58, (1985) 1.
12. Picone, P.J. J. Crystal Growth 87 (1988) 421.Tanguay, A. Jr. Optical Eng'g. 24 (1985) 002.
13. Duffar, R. et al., J. Cryst. Growth 100 (1990) 171
14. Foldari, I., Opt. Mats. 2 (1993) 25.Grabmaier, B.C, et al, Phys. Stat. Solidi (A) 96 (1986) 199.
15. Larkin, J., J. Crystal Growth 128 (1993) 871. Valley, G.C., Ann. Rev. Mats. Sci. 18 (1988) 165.

## Relevant current work in support of this project:

Most recently focus at the EML was placed on growth and characterization of electro-optic materials where further advances in related device technologies are recognized as primarily contingent on progress in crystal growth and defect engineering. The similarity of defect structures in these materials and in semiconductors suggests the applicability of analog approaches in efforts to advance our understanding of growth, segregation and defect formation; it accentuates furthermore the appropriateness and potential benefits of

experimentation in a reduced gravity environment. NASA sponsored, ground-based research was for this reason redirected towards:

## 1. Identification of an electro-optical materials system that can be considered representative for photonic materials.

That is also of (a) technological relevancy, (b) has a credible, established data base and (c) is amenable to meaningful μ-g crystal growth studies with a minimum of instrumental complications.

**The system of choice is: Bismuth silicate - $Bi_{12}SiO_{20}$ - (BSO)**

### Thermophysical properties of BSO

| Quantity | Temp. (K) | Value |
|---|---|---|
| Melting point | 1168 | |
| Density (s) | 293 | 9.206 $g.cm^{-3}$ |
| Density (l) | 1223 | 7.63 $g.cm^{-3}$ |
| Linear exp. coeff. | | $1.6x10^{-7}$ $K^{-1}$ |
| Volume exp. coeff. | | $7x10^{-5}$ $K^{-1}$ |
| Specific heat (s) | | 2.7 $J.cm^{-3}K^{-1}$ |
| Specific heat (l) | | 3.0 $J.cm^{-3}K^{-1}$ |
| Thermal cond. (l) | 973 | 0.1944 $W.m^{-1}K^{-1}$ |
| | 1073 | 0.1782 $W.m^{-1}K^{-1}$ |
| | 1168 | 0.162 $W.m^{-1}K^{-1}$ |
| Thermal cond. (s) | 1168 | 0.27 $W.m^{-1}K^{-1}$ |
| Viscosity | 1173 | 0.22 $dyn.cm^{-2}s$ |
| Breaking strain | | $2x10^{-4}$ |
| Latent heat | 1168 | 460 $J.cm^{-3}$ |

Phase diagram of BSO

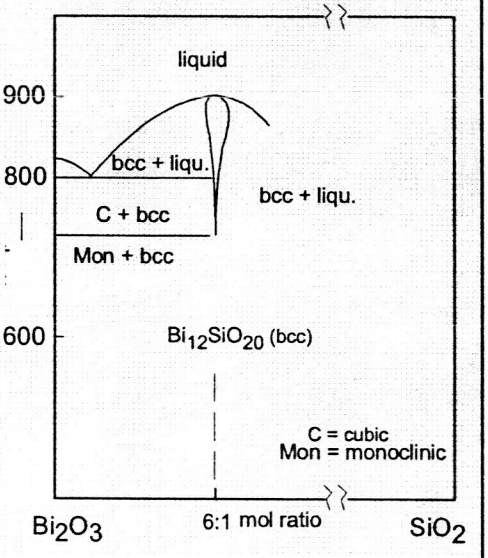


BSO, a member of the sillenite family (1), exhibits outstanding piezoelectric properties and exceptionally high rotative activity. It is also photo-conductive and has a linear electro-optical effect which makes it suitable for optical as well as microwave and surface-wave acoustic applications. The full potential of this material, demonstrated in property measurements, has however so far not been realized in device applications primarily because the degree of control over crystalline and chemical perfection achievable to date by conventional growth techniques is inadequate to produce devices with acceptable performance characteristics. Stoichiometry control, uniform dopant incorporation on both a micro- and macro-scale, facet growth with related segregation and stress effects as well as confinement related contamination remain unresolved issues.

From theoretical considerations and from results of melt growth experiments in a reduced gravity environment, it is concluded that with the reduction of gravitational forces the degree of undesirable convective interference with growth and segregation will be significantly

reduced as will be the interaction between the melt and its confinement. Crystal growth of BSO in a virtually unconfined mode, desirable for minimization of stress and confinement related contamination, is considered a possibility.
The selection of BSO as a test material is based on two primary arguments:
(a) The electro-optical activity in BSO is not inherent; rather, it is attributable to the presence of a high density of defect states:

"The defect concentration in BSO single crystals is large, ranging up to about $10^{19}/cm^3$. Growth related fluctuations in the distribution of these defects create local potentials, internal fields which give rise to recombination barriers and long and varying recombination times."

The results of uncontrolled defect formation are limitations in the yield and performance of devices. Realization of the true potential of photo-refractive materials in devices appears thus contingent on adequate control of defect generation during crystal growth. It is contingent on effective defect engineering for which (as stated above) the foundation can best be established through expermentation under conditions of reduced gravitational interference with growth.
(b) BSO's relatively low melting point (1168 K) permits the use of conventional heat-pipes as liners for heat transfer control in furnaces. Heat-pipes will facilitate the establishment of reproducible and quantifiable thermal boundary conditions for growth and thus render the application of computational approaches to both, analysis and control of the growth process more meaningful.

## 2. Development of a Czochralski type crystal pulling system for oxides

With (a) a heat pipe based hot zone, (b) ambient composition and pressure control and (c) current induced growth interface demarcation capability.

A Czochralski-type crystal growth system for BSO with controlled ambient has been constructed (3). The system uses resistance heating and an Inconel heat pipe installed coaxially about the (Pt) crucible containing the charge to provide for a virtually axi-symmetric, controllable thermal environment; the growth environment is separated from the heater and the heat pipe by a coaxial quartz glass cylinder to permit growth under controllable partial pressures of oxygen. Thus the charge can be maintained in an oxygen-containing atmosphere while the heat pipe and heaters operate in a protective inert atmosphere of argon. Provisions are made in the system for application of current induced growth interface demarcation. Demarcation during growth was achieved with pulses of 25 mA at potentials (V) ranging from 25 to 200 Volt at the beginning and late stages of growth (5 cm) respectively.

Using seeds of <100> orientation, single crystals at diameters of up to 2cm have been grown (at pulling rates ranging from 0.5 to 1.5 cm/h with seed rotation rates of 10 to 30 rpm) from undoped and Ga-doped charges of 30 to 70g (in Pt crucibles) with nominal composition of $Bi_2O_3$:$SiO_2$ = 6:1.
In growth experiments it was found that the oxygen partial pressure in the ambient has a pronounced effect on the morphology of the growing crystal. During growth with constant power input an increase in the partial pressure of oxygen from 10 at/o to 100 at/o was found to result in the disappearance of external faceting, in a pronounced decrease in crystal diameter and in a noticeable increase in the density of (as yet unidentified) gas phase inclusions. (This finding is contrasted by the growth behavior of $LiNbO_3$ reported earlier (4).

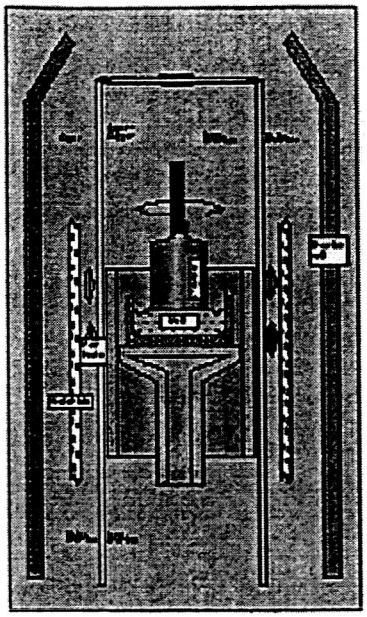

Figure 2-1. The Czochralski type crystal pulling system for BSO growth.

The Czochralski growth facility was used to provide material for the deelopment of growth related chemical and structural defect analyses, to establish the capability for generation and detection of current induced growth interface demarcation in BSO to investigate platinum - melt interaction in the presence and absence of potentiostatic polarization, and to supply crystal seeds and charges for the development and characterization of a Bridgman type growth facility.

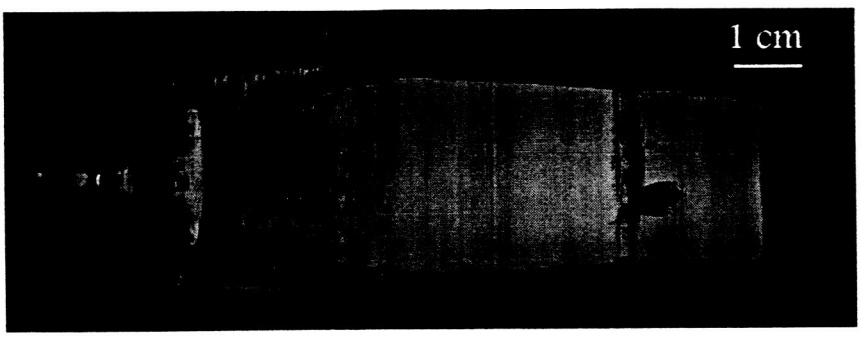


Figure 2-2. Chochralski growth crystal. Top and bottom contained a number of mactoskopic defects but center section optically clear.

## 3. Development of a vertical Bridgman type crystal growth system

A heat pipe based vertical Bridgman-Stockbarger crystal growth system has been developed which provides for quantifiable and controllable boundary conditions with radially symmetric thermal field distribution. The system also permits -stabilization of the crystal melt interface position, growth at fixed axial thermal gradients and is compatible with the hardware infrastructure of NASA's CGF system. The adopted configuration, based on the Bridgman-Stockbarger geometry used axially aligned heatpipes (0.88"ID) with Li as heat transfer fluid. The heat pipes, functioning as hot and cold zones, respectively, are separated by a gradient zone of adjustable height (currently set at 2.5") To provide for stabilization of the growth rate during crystal growth (ampoule displacement) the temperature controlling T/Cs were relocated from their customary hot and cold zone locations to the gradient zone and positioned at 2 cm vertical spacing above and below the desired location of the growth interface. This arrangement of the temperature controlling sensors is designet to a) provide for stabilization of established axial thermal gradients during all stages of growth and to b) minimize growth rate transients related to changing charge position associated with continuing growth (changes in thermal coupling between furnace and charge) through compensating changes in input power,

It is suggested that this B-S system provide the basis for the ground based research program and as desired feedback to the design of the growth system on ISS. The requirement of a Pt liner for charge confinement does preclude the application of current pulsing for interface demarcation in ground based experiments. Verification of the functionality of the heat pipes (equality of the growth rate with the charge displacement rate, establishment of radially symmetric growth interface morphologies) is therefore to be established (at decreased resolution) through thermal pulsing and the post-growth identification of related growth striations. which are revealed through interference contrast microscopy (reflection mode) in the wavelength range from 450 to 500 nm.

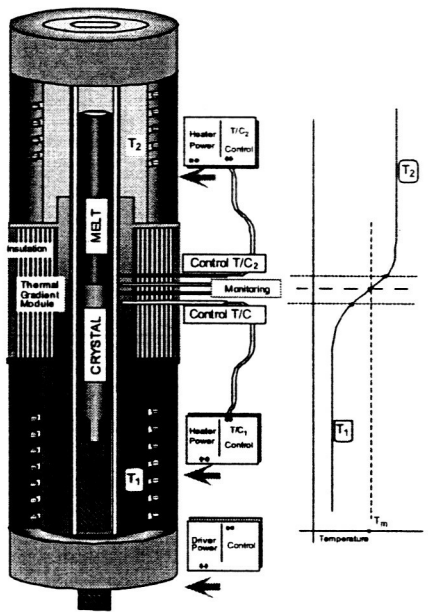


Fig.3-1 Heatpipe-based Bridgman-Stockbarger growth system with crystal-melt interface stabilization.

The use of heat-pipes in the design of the Bridgman system is considered essential since thermal boundary conditions of conventional heater systems are neither radially uniform, nor

adequately quantifiable and reproducible. [It must also be mentioned that commercial heat pipes used in this laboratory have been in operation at temperatures of up to 1300K for in excess of 500 hours without unprovoked failure; they must not be considered a safety hazard in space operations since, in addition, the vapor pressures of the heat transfer medium (Na or Li) at BSO growth temperature are only 1 atm and about $10^{-2}$ atm respectively.]

During thermal characterization of the B-S furnace with a dummy boron nitride charge, it was found that all critical thermal parameters performed as expected. Of primary interest is the finding (see figure 3-2) that, inserting the dummy without a Pt confinement-reflector, in no horizontal position within the gradient zone could the growth interface morphology of the dummy charge be reversed from concave to convex. (the peripheral temperature in the dummy remained lower than that in the center at all horizontal positions within the gradient zone.) Such a growth interface morphology reversal could be achieved reproducibly on insertion of the (0.08 mm thick) Pt confinement foil.

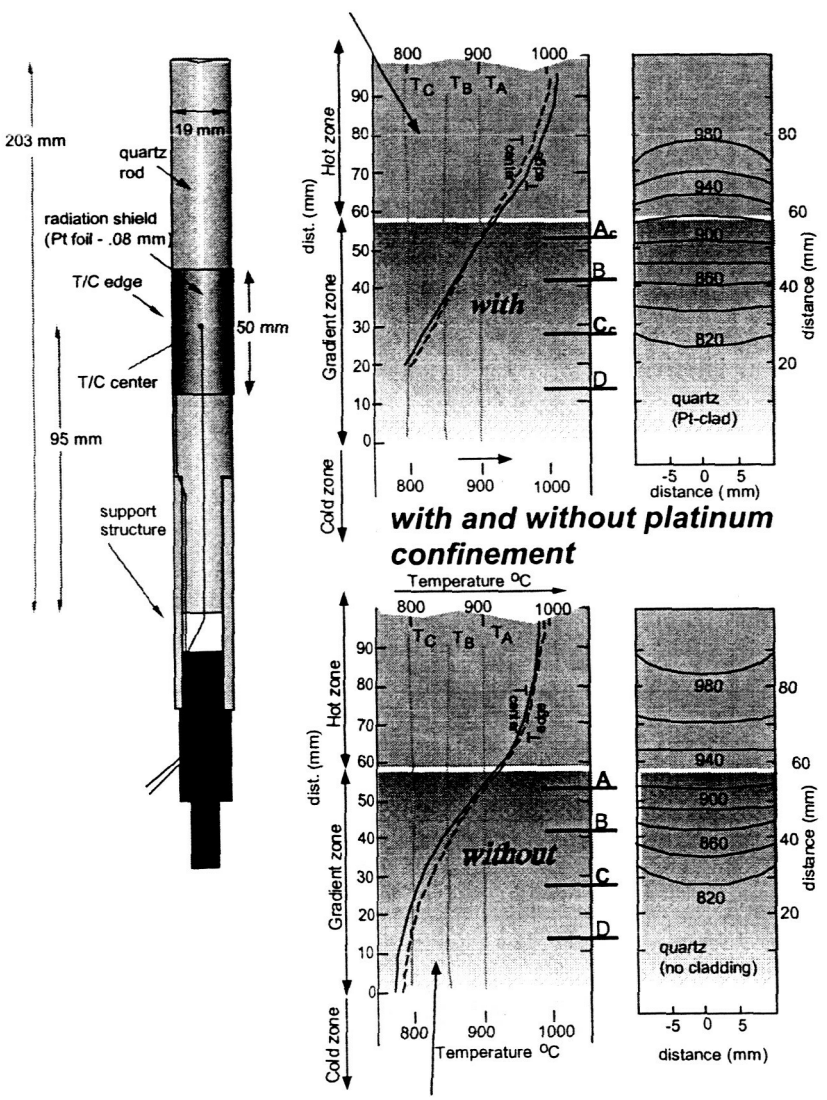


Fig.3-2 Thermal characterization of Bridgman-Stockbarger furnace with and without a Pt liner, required during growth of BSO of 0.08 mm thickness.

Charge confinement issues: The confinement (crucible) system for BSO must provide for accommodation of a seed, reproducible geometry, chemical compatibility with the charge and minimized conductance along the crucible wall. Because of the corrosive nature of BSO melts, the objective of charge confinement could in principle best be met through the use of an appropriately shaped platinum ampoule.

Experiments showed, however, that such crucibles without support structure are substantively deformed during removal of grown crystals and thus preclude reproducibility of growth conditions; vacuum deposited Pt liners and Pt paint liners in silica shells exhibited pinholes and inadequate adhesion respectively

A surface analysis of the Pt foil (from the prime supplier) used for confinement revealed, pronounced thickness variations, as well as extensive work damage. Integrity of effective confinement is not assured, nor is reproducibility of confinement conditions.

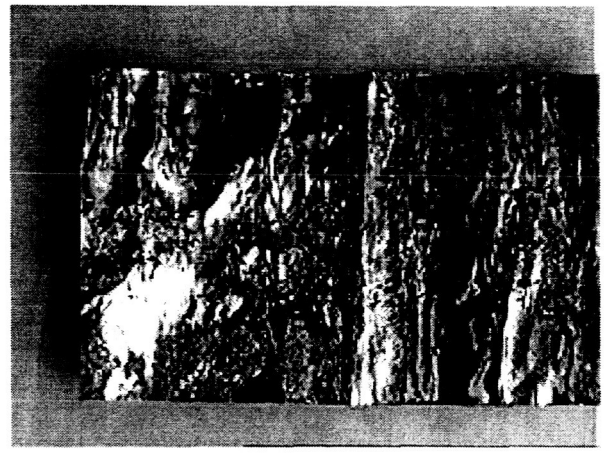

Figure.3-3 Platinum confinement following growth and after removal from quartz ampoule; randomly distributd particles of BSO observed on both sides as well as corrosion; (x 15)

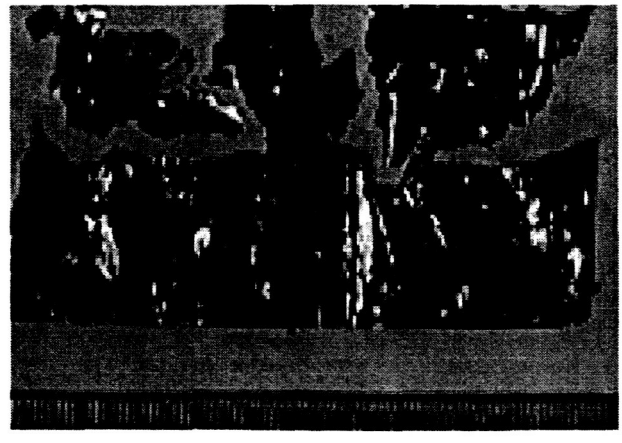

Fig.3-4 Failure of confinement material, diagnosed as a result of deficient quality control during manufacture of the foil (x 15)

Since it has been established that the wetting behavior of molten charges in space, is not predictable from charge confinement interaction in ground-based experiments, KC-135 experiments were conducted to get to extract guidance from intermediate g experiments: Short duration growth experiments under reduced g conditions ($10^{-2}$) did not reveal any marked differences in the wetting behavior of the melt.

Considering the inability of the supplier to achieve improved foil thickness control, further consideration is given to thin film deposition and to increased "safety margins" in thickness. If confinement foil is to be used in space experiments, the thickness requirement is increased from .08 to .35 mm.

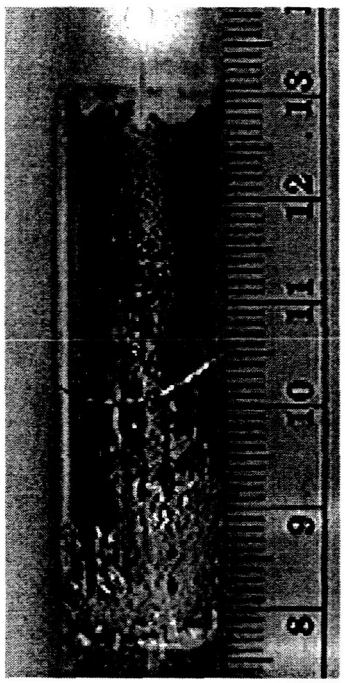

Fig. 3-5 Growth ampoule with solidified charge as removed from the B-S system (crack in glass was accidental). The crystal within was found to be "single" over 2/3 of the growth length; condensate, predominantly $Bi_2O_3$, is attributed to condensation.

**Growth and Analysis of Bridgman-type BSO:**

In standard procedure, B-S growth makes use of a seed and a poly crystalline perform (or a centerless ground Cz crystal) as charge which are inserted with the confinement foil into the quartz ampoule. After flushing with oxygen the ampoule is evacuated and refilled with a predetermined oxygen gas mixture to atmospheric pressure and growth is conducted "open" in an ambient of pure oxygen or synthesized "air" or alternately in the sealed ampoule with RT pressure no to exceed .5 atm. The ampoule is inserted into the furnace to the desired position, gas flow is initiated, the temperature raised in a pre-programmed manner and the charge lowering cycle activated.

After growth, the sample is oriented to XRD, cut with a string saw to specifications and after lapping was polished with a Syton solution.

First analysis was conventionally done by interference contrast microscopy in either reflection or transmission mode. A micrograph of a segment of the crystal above is shown in fig.3-7. It reveals the presence of intensive "deep trap striations" in the seed portion and the virtual absence to optical non-uniformities in the portion grown by the B-S technique. The same, undoped crystal, when viewed in transmission mode (white polarized light) reveals oriented, likely stress induced, dislocation networks and minor precipitates. Fig. 3-7

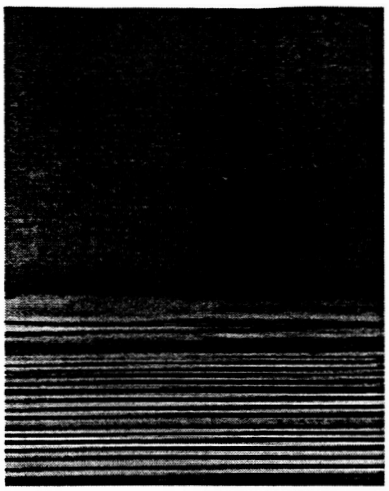

Fig.3-6 Interference contrast micrograph (x 160) of undoped BSO grown by the Bridgman-Stockbarger technique; notice the absence of optical inhomogeneities which characterize the seed material, grown by the Czochralski process.

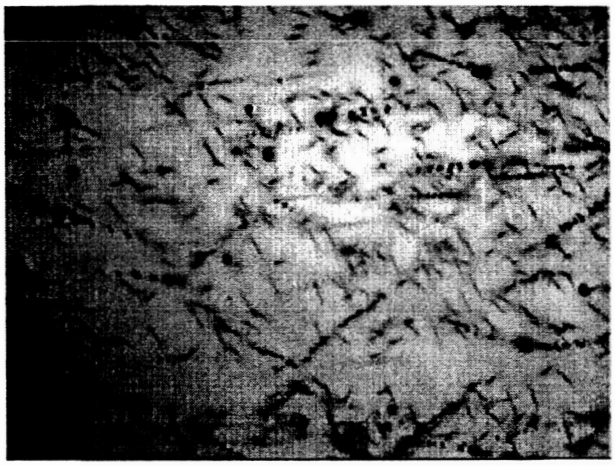

Fig.3-7 Dislocation net work in Bridgman type BSO crystal (x 230)

Of interest in context with the projected research program, is the appearance of optical heterogeneities in the form of low intensity striations (Fig.3-8) observed in a multitude of Bridgman type crystals. This finding suggests that, although their driving forces must be considered as minimal according to established criteria, convective flows prevail in vertical Bridgman configurations.

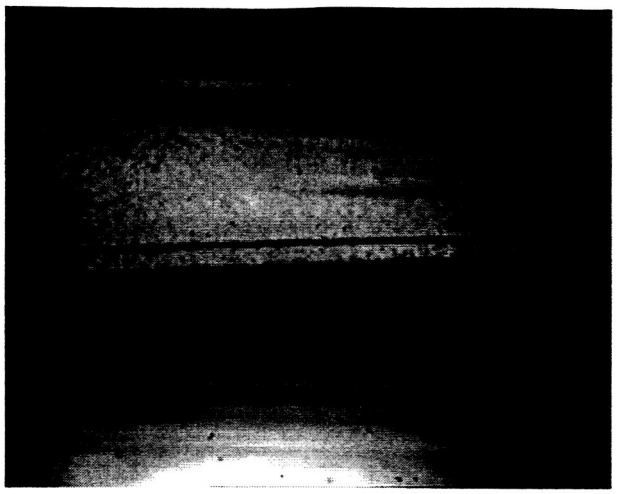

Fig.3-8 Chromium doped Bridgman-type single crystal exhibiting precipitates as well as striation like optical heterogeneities, suggesting residual convection (x 90)

Our finding of convection, interfering with growth and segregation, in Bridgman-type growth of BSO is contradicted in findings reported by Xu et al. They report the absence of convection during Bridgman growth of doped BSO, based on chemical analysis of two crystal samples, one each from the head and the tail and assume applicability of the Jackson – Tiller segregation analysis, obtaining computed interface segregation coefficients with 4 significant figures; data discrepancies are explained as evaporative losses. The justification for assuming a convection free environment in their growth experiments is, in addition to their chemical analysis, published work by Clayton et al and by Rouzaud et al.

Since the answer to presence or absence of convection during Bridgman-type crystal growth has of fundamental implications on the conduct of the projected research program, the cited work was analyzed and the conclusions of Xu at al were found to be at variance with the evidence. Considering the finite slope of the composition diagram, convective interference with the solute boundary layer must be assumed. (It should be noted that some of the authors of the cited work, later published work on magnetically stabilized Bridgman growth of HgCdTe and reported achievement of a flat segregation plateau.)

An analysis of the published work by Rouzaud [lit] on growth of Si-Ge alloys as well failed to confirm the conclusion of convection free growth.

A comprehensive study of published experimental results on growth and segregation in vertical Bridgman-Stockbarger geometries provides no verifiable evidence for the establishment of convection free growth conditions. The sole most credible evidence of B-S crystal growth with the virtual absence of convective interference is provided in unpublished results of Lichtensteiger, involving growth of Ga doped germanium on the space shuttle.

## 4.The phase diagram of BSO ($Bi_{12}SiO_{20}$) and characteristics of native defect formation:

$Bi_{12}SiO_{20}$ is isomorphous with $Bi_2O_3$ which in turn is polymorphous. The BSO phases of concern are: the ("impurity stabilized") high temperature, cubic body centered $\gamma$-phase and the (apparently ) stable (face centered cubic) high temperature $\delta$-phase. The complete phase relations and crystallizing behavior of the $Bi_2O_3 - SiO_2$ system are as yet neither fully explored nor completely

understood. The most comprehensive study of phase relations for a member of the Sillenite family was conducted by Corsmit et al for BGO (it includes a contribution to the phase regions in the molten state by Tananaev ). A more limited number of phase data on bismuth silicate (BSO) have been published by Takamori and by Kargin ] (Fig.4-1).
The issues of primary concern in context with this review is the congruent melting point, the absence of extended existence region and the existence of definable phase fields in the melt region.

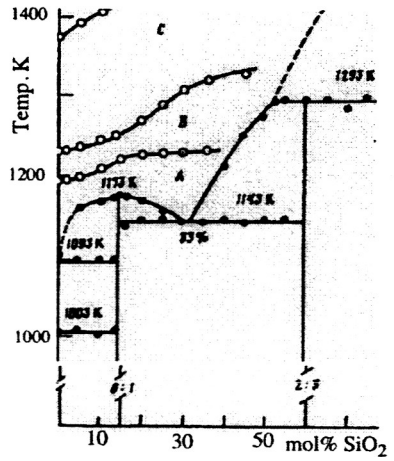


Fig.4-1 Phase diagrams for the systems $Bi_2O_3$-$SiO_2$ covering the bismuth rich side. [Tananaev]

The publication of Kargin et al, is focused heavily on the appearance of structured species (clusters) in melts of BSO and BGO. Identification of the related phase fields (A), (B) and (C) in figure 38 is based on measurements of the functional dependence of melt density and viscosity on temperature and composition (Fig. 4-2) .

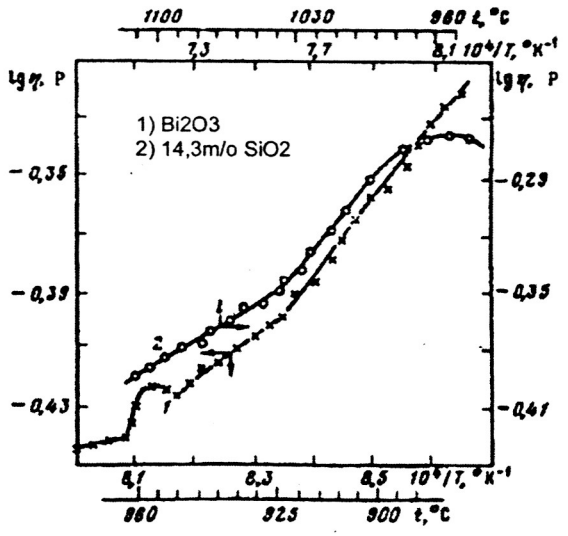


Fig. 1

I.Tananaev et al.

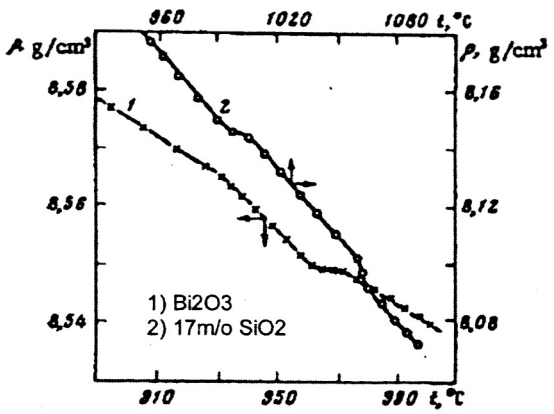


Fig. 2

Fig.4-2 Viscosity and density polytherms of melts in the system Bi2O3-SiO2.

Their data suggest that structural changes in the melt (temperature dependent "clustering")

lead to the formation of different species, subdividing the temperature field into three regions extending respectively from the melting point to about 925°C (A), from 925 to 1020°C (B) and beyond 1020°C (C).

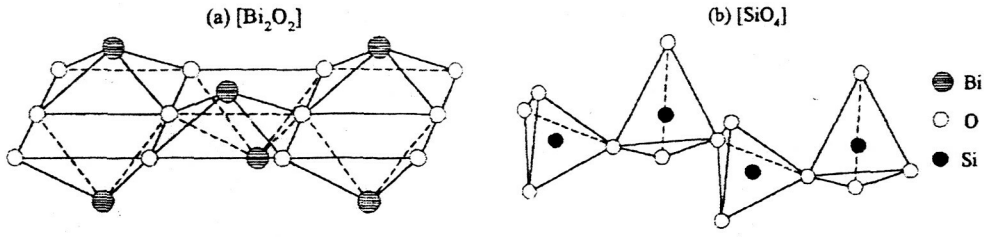


Fig. 4-3 Proposed cluster configurations formed in BSO melts at temperatures ranging from about 950 to 1020°C (zone B). [Zhereb]

Tananaev (1979) states: "Cooling of BSO melts from zone B (temperature range from 950 to 1020°C) leads to crystallization of metastable phases (d-phase) without incandescence and with significant supercooling.; with excellent mixing (crucible rotation) metastable phase crystallized even at cooling rates of 50° /min; without mixing, at that cooling rate we obtained a stable phase with spontaneous incandescence."

(It should be noted that the phase identification was reportedly done by XRD and is unambiguous. The validity of the density and surface tension data obtained by the authors, however,
is questionable since they are based on sessile drop measurements. Such measurements, also conducted in this laboratory in context with wetting experiments of BSO melts on platinum, revealed significant deficiencies. Basic assumptions related to the computational determination of thermodynamic data from sessile drop shapes are not met: (a) drops are not axi-symmetric, (b) contact angles are subject to substantial hysteresis, (c) drop boundaries are not circular and reflect grain boundary pinning.)

DTA and XRD measurement on BSO specimens originating from melts subjected to quenching and controlled cooling, respectively [Takamori (1990), Fu et al (1996)], appear to confirm the basic findings of Tananaev.

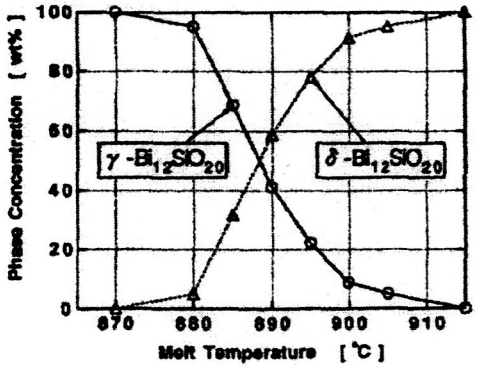


Fig.4-4 "Phase concentrations of BSO as a function of melt temperature prior to $H_2O$ quenching [Fu1996].

Accordingly, the phases forming on solidification of BSO melts, either metastable δ-$Bi_{12}SiO_{20}$ or of stable γ-$Bi_{12}SiO_{20}$ or both, appear to be dependent on both the maximum melt temperature and the cooling rate: high melt temperatures and cooling rates tend to result in metastable δ–phase; formation of δ-phase is suppressed and g-phase is formed from melts at temperatures

of less than 935°C [Fu 1996]. The non-linear temperature dependence of viscosity and density in BSO and BGO melts, the basis of the clustering theory, is negated by Shigematsu et al (1994).

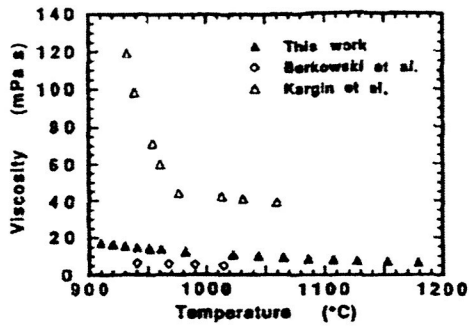


Fig.4-5 Temperature dependence of the viscosity of BGO melt [Shigematsu 1994]

The authors report for BGO ($Bi_{12}GeO_{20}$) a linear relationship between viscosity and 1/T indicating that the activation energy for viscous flow is constant over the indicated temperature range and that the fundamental melt structure remains the same; according to their findings, there is no indication of cluster formation. The authors report further that their results are in agreement with EXAFS spectra obtained by Omote et al (listed as: in press; citation could not be found by ScienceFinder).

**5. Development of characterization techniques for crystalline and chemical defects in bismuth silicate and means for the detection of growth interface demarcation.**

In view of long term preoccupation and experience in optical characterization gained from ARPA- and NASA-sponsored research of III-V and II-VI compound semiconductors, existing comprehensive facilities for optical microscopy and related computational image processing were analyzed for applicability to defect characterization in BSO.

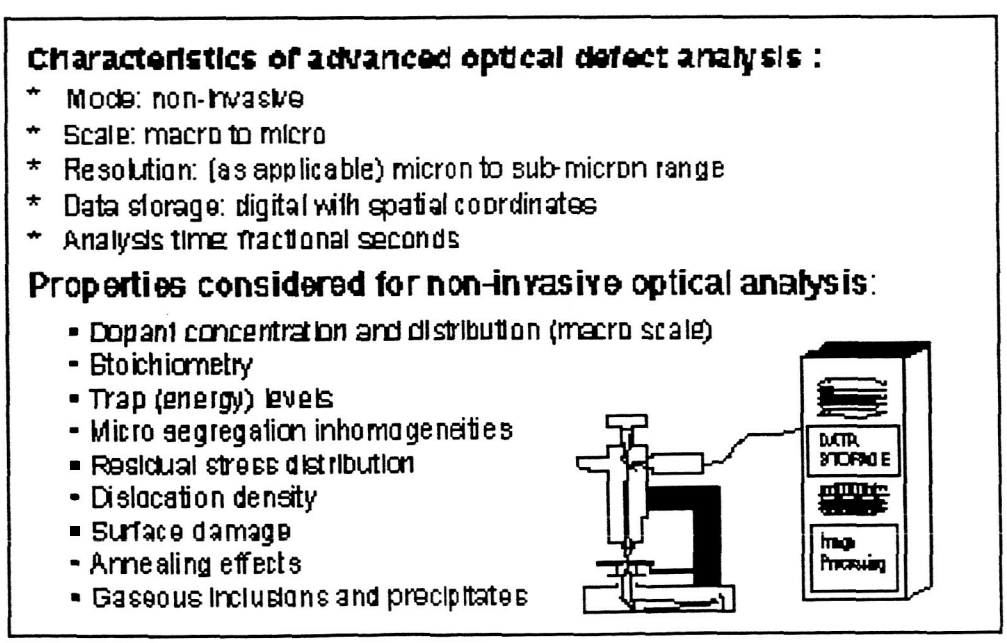


Figure 5-1. Characteristics of optical defect characterization with computional.

BSO crystal segments (~ 1cm thick) of desired location and orientation were cut using a string saw, mounted with crystal bond on brass disks, and subsequently lapped and chem-mechanically polished on both sides with Syton solution. Analyses were carried out using bright field, dark field and phase contrast transmission microscopy on a Zeiss Axiotron and an Ultraphot. Imaging was accomplished using a Dage MTI SC-70 vidicon and alternately a Sony CCD camera. The images were digitized into an array of 512x480 pixels with 256 gray level resolution and were stored in a host computer for further processing and/or analysis (7).

Examination of nominally undoped segments of single crystals by transmission microscopy finds them to be yellow to orange, exhibiting faint banding of periodicities other than expected for rotational striations. To ascertain information on energy levels associated with the defects responsible for the banding effect, optical absorption spectra were determined. The spectra revealed substantive broadening of the optical band edge, an effect which was anticipated from findings in earlier studies.
Under the assumption that defect (energy) levels located at the band edge are irresponsible for the appearance of optical striations, samples were viewed with filtered illumination using a narrow band pass filter centered at 450 nm (±10 nm).

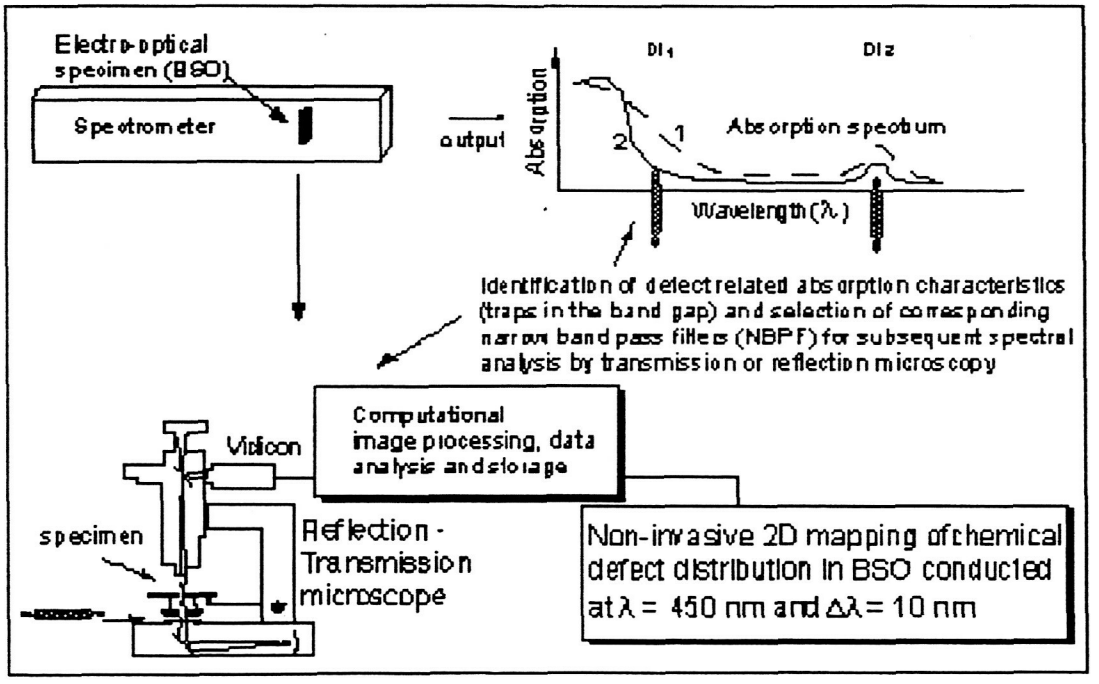


Figure 5-2. Approach to defect analysis in BSO based on spectral absorption analysis and interference contrast microscopy (in transmission and reflection mode) using selected (narrow band pass filtering) monochromatic radiation.

In transmission microscopy, striations were observed with markedly increased contrast and thus permitted quantitative examination. It was found that:

(1) Conventional, rotational striations are absent in both doped and nominally undoped BSO crystals; this finding is attributed to heat pipe action which to provide for radially symmetric thermal field distribution;

(2) Non-rotational striations, highly periodic in nature and exhibiting two distinctly different frequencies, are present in both the core and off-core regions; neither frequency was found to correlate with power fluctuations;

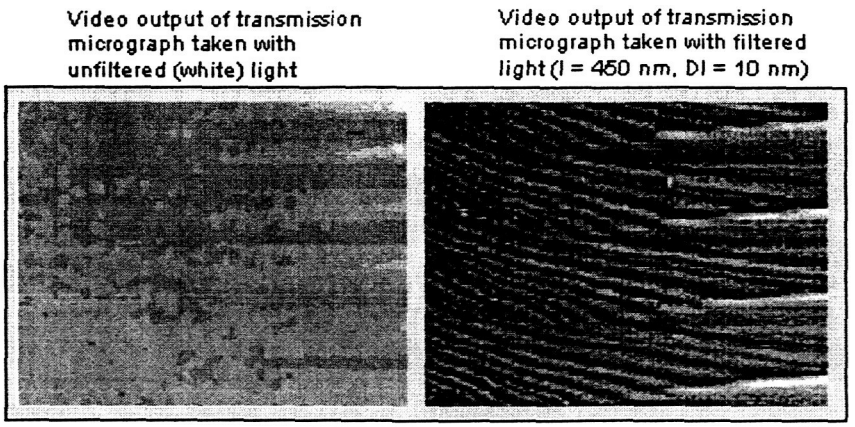


Figure 5-3. Spectral analysis of "striated" distribiution of deep level defect in nominally undoped BSO.

(3) The frequency of striation formation appears to be a weak function of the aspect ratio of the charge, independent of the rate of seed rotation and not noticeably dependent on the rate of crystal pulling; preliminary analyses in commercial crystals indicate spacings of defect striations in core and off-core regions ranging from the limit of resolution (0.6 μm) to several tens of μm.

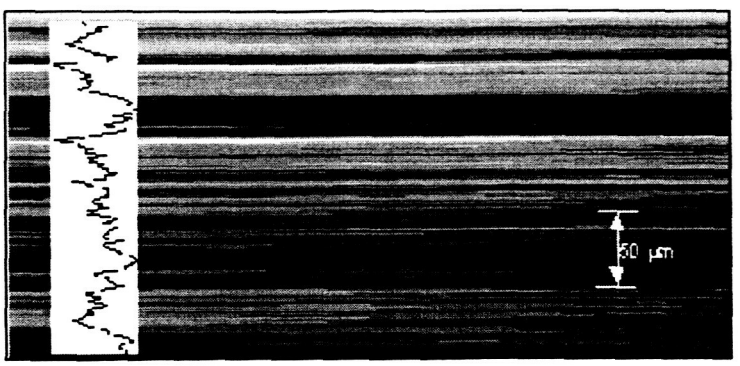


Figure 5-4. Striation analysis in BSO using interference contrast in reflection mode and filtered radiation.

(A) Pronounced off-core striations in the "shouldering region", the transition after seeding, from increasing to constant crystal diameter. The observed pattern reflects seed rotation during a period of bulk melt-flow reversal.

(B) Absorption inhomogeneities in faceted (core) regions at spacings which approach, and likely exceed the optical resolving power of the microscope; they remain in focus on moving optically through the crystal segment, suggesting a two-dimensional defect of limited lateral extension.

(C) Interface instability effects in formally undoped, commercial BSO

(D) Rotational off-core striation in undoped, commercial BSO

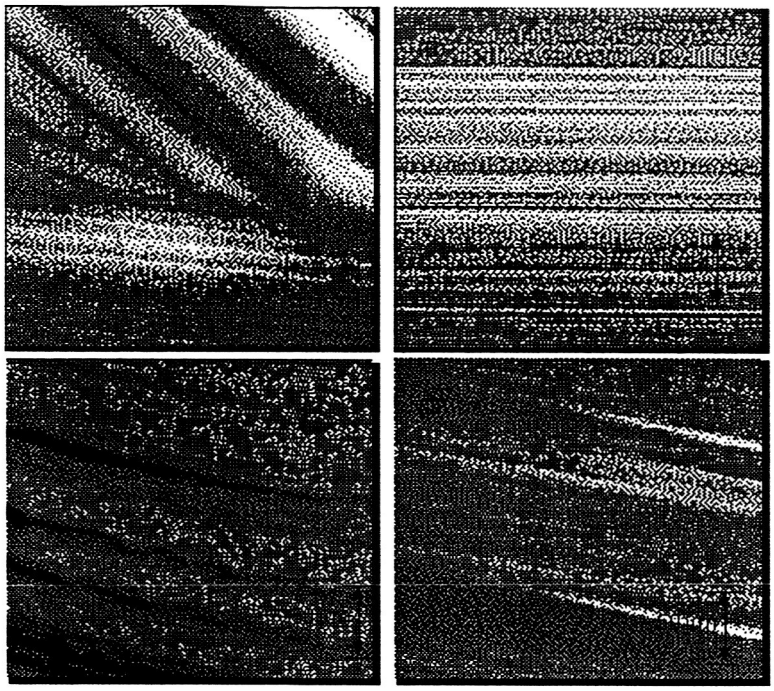

Figure 5-5. Spectrum of optical absorption inhomogeneities in commercial BSO, observed with interference contrast microscopy in reflection mode (at $\lambda$ = 550 nm) upon computational contrast enhancement.

(4) The primary macroscopic crystal deficiencies are precipitates and gaseous inclusions; their appearance is found to be a function of the rate of crystal rotation, the rate of crystal pulling and the oxygen partial pressure in the ambient;

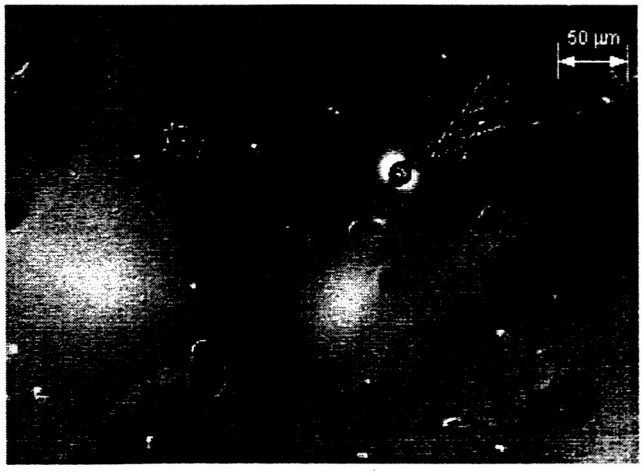


Figure 5-6. Gas inclusions and precipitates in BSO; the exact nature of these prononceted scattering centers is still subiect of controversy

(5) Current induced interface demarcation has been applied during Cz growth. Neither demarcation lines nor conventional striations could be revealed by chemical etching

procedures; they could, however, be observed by transmission microscopy using "monochromatic" illumination. The characteristics of demarcation lines, generated with current pulses ranging from 10 to 25 mA, were identical for both current polarities which led to the conclusion that their origin is not attributable to a Peltier effect, as is the case in semiconductors.

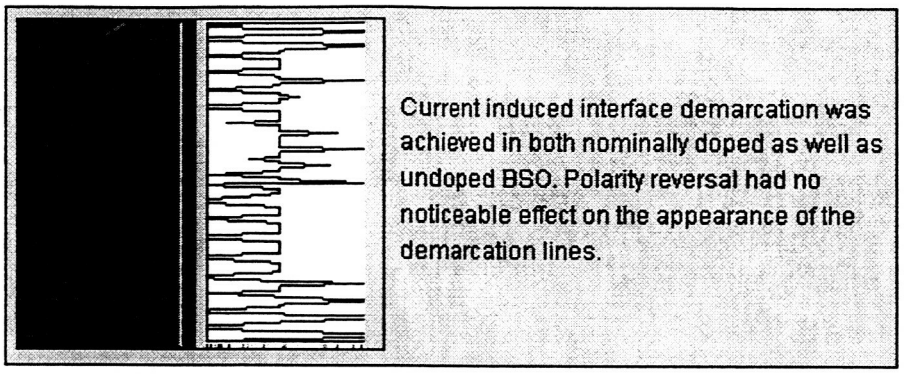


Figure 5-7. Current induced interface demarcation in BSO as revealed by transmission microscopy using light centered at 450 nm with $\Delta\lambda$=10 nm.

The presence of dislocations in BSO was deduced from the appearance of "etch pits". The identity of the pits as dislocation etch pits could be established by subjecting crystal segments at 600°C to thermal anneal in a reducing ($H_2$) atmosphere. Under these conditions the dislocations become "self" decorated and visible in transmission microscopy (8).

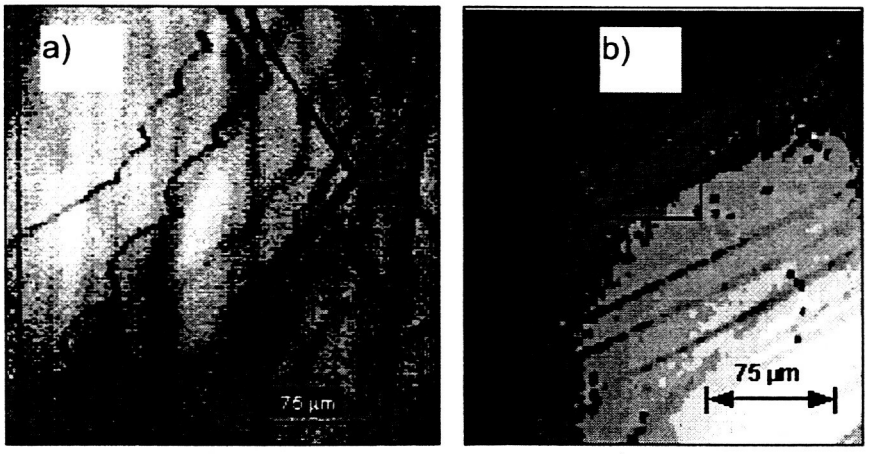


Figure 5-8. a) Dislocation network in BSO as observed in conventional transmission microscopy after a reductive anneal at 600 C., b) Etch pits and corresponding dislocations in BSO as revealed in transmission after reductive anneal at 600 C.

**Literature:**

1. Speranskaya, E.I., Neorg. Mater. 4 (1968) 1374
2. Attard, A.E., J. Appl. Phys. 66 (1989) 3211
3. Lin, Chenting: Crystal growth and characterization of $Bi_{12}SiO_{20}$. MIT,DMSE,Thesis, 1995

4. Shigematsu, R., J. Appl. Phys. 140 (1992) L582
5. Papa Rao, Satyavolu, S.: Control of growth interface location and morphology in a heat pipe based vertical Bridgman system. MIT, DMSE, Thesis, 1996
6) Papa Rao, S.S. et al. J. Cryst. Growth (submitted for publication)
7) Lin, C. et al. J. Cryst. Growth (submitted for publication)
8) Lin, C. et al. J. Cryst. Growth. 140 (1994) 444
(a) Petrova, D., Gospodinov, M., Sveshtarov, P.: Optical absorption of photorefractive $Bi_{12}SiO_{20}$ crystals doped with Zn, Cd and co-doped with P. Cryst. Res. and Techn. 31 (1996) 577

## 6. Development of characterization techniques for measurement of the Photorefractive Effects

The "Photorefractive Effects Measurements System" was dedicated in Memory of Professor August F. Prof. Witt was the initiator and original Principal Investigator of this research project.

Fabricated equipment is currently used for: recording and read-out of holograms, beam coupling gain, and signal processing response time measurements.
The Photorefractive effect is a result of a light-induced change in refractive index. It is a third-order nonlinear effect allowing for the recording of a holographic grating in response to the interference of two monochromatic (Argon laser) light beams. Read-out of the recorded holograms is performed through the diffraction of a weak probe beam (HeNe laser) at Bragg conditions. The PR-Effects measurement system is assembled on a optical table.
Figure 6-1 shows the layout of the Photorefractive Effect Measurements System.

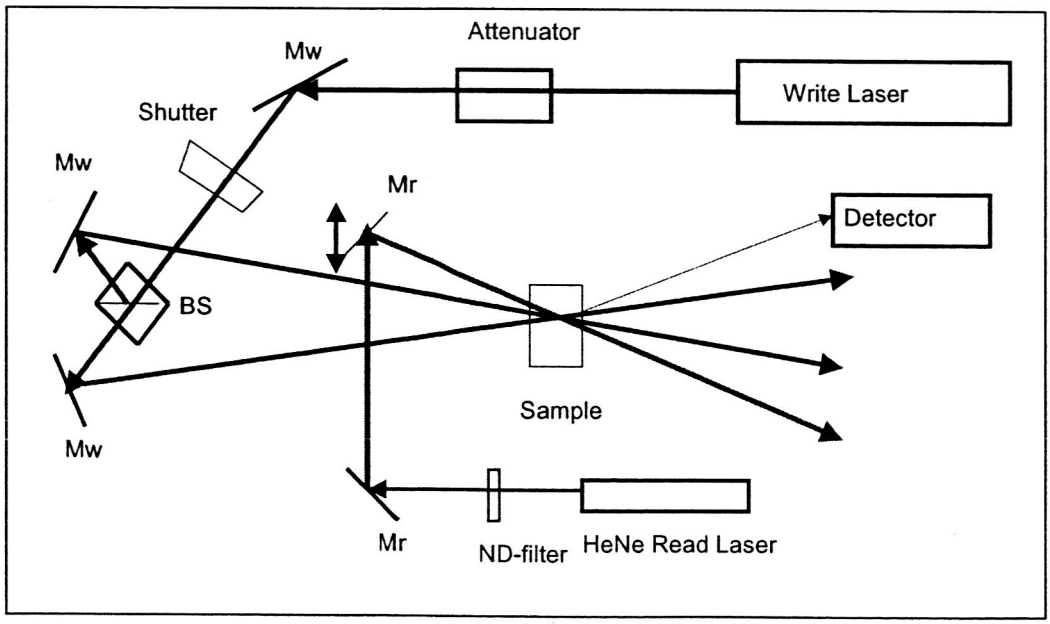


Figure 6-1. The photorefractive effect measurement system layout.

Write Beam.

The write laser is a Melles-Griot multi-line air-cooled Ar laser with a prism setup to select the desired laser line (488 or 514 nm).
The attenuator is made from two polarizing cube beamsplitters. One is mounted in a rotating holder the other fixed. The laser is vertically polarized and the fixed output beamsplitter is mounted for vertical output.
Mw stands for mirrors in the write-beam. In our system the two nearest the laser are elliptical while the two near the beamsplitter are 2 inch diameter circular mirrors. For simplicity in ordering all can be circular. Of course, they need to be front-surface. We use precision mounts from both Newport and MellesGriot with the adaptors needed to hold them on the 1.5" dia. X 12' tall posts. If I were setting it up from scratch again I would consider using magnetic bases (Edmund A39-926) with appropriate blocks to hold the mirror mounts. The magnetic bases would make it easier to position the mirrors. Posts make vertical positioning easier. Use good mirror mounts. Ours have micrometer adjustment screws, the micrometer readings are never used. Newport (and others) now sell mounts with better screws. The finer the screw the easier it will be to align. Note: the screws in Edmund mounts are a bit marginal.
The beamsplitter is a 25 mm nonpolarizing cube beamsplitter. We bought ours from MellesGriot. Edmund now sells them as well. It is mounted on an Edmund magnetic base with an adjustable prism holder.
The shutter is from JML with their controller. I think Uniblitz sells a nearly identical shutter. The controller has a serial interface so it can be controlled by the computer.

The Read-Out Beam.

The HeNe read-out beam needs to be at the Bragg angle for the grating. We started out using a laser mount from MellesGriot that allowed us to move the laser for aiming. This did not work very well. We then went to a system where the laser is rigidly mounted parallel to an edge of the table. Our current setup is shown in Fig. 1. The first mirror aims the beam across the table. Once it is positioned in the center of the HeNe beam only the angle needs to be adjusted. The mount has adjustments for horizontal and vertical angles. The second mirror also has horizontal and vertical angular adjustments and is mounted on a translation stage so that it can be moved fairly precisely in the direction indicated by the double arrow. The vertical angle adjustments allow the read beam to be vertically centered on the crossing write beams. The horizontal angle adjustments allow the read beam to be set to the Bragg angle while the translation stage allows the read beam to be centered on the crossing write beams without changing the angle. A neutral density filter screen is used to set the intensity of the read beam. These filters can be obtained from Edmund or MellesGriot (and others). Our HeNe is a 6 mW (new – no about 5 mW after 10 years) vertically polarized laser. A lower power HeNe could be used but it should be polarized.

Setting the angles.

We normally use a 2 micron grating spacing. In setting things up we usually end up with a spacing between 1.9 and 2 microns. It does not seem to be critical for our experiments. We determine the write-angle, $\theta_w$, by measuring the distance, $D_w$, between the two write

beams 24 inches from the sample (on the outgoing side). Then $\sin\theta_w = 0.5D_w/24$ using the small angle approximation. Note, many authors give the crossing angle which is $2\theta_w$. The grating spacing, $\Lambda$ is then given by $\Lambda = \lambda/(2\sin\theta_w)$. Where $\lambda$ is the wavelength of the write beams. The Bragg angle, $\theta_B$, is then found from the usual formula $\sin\theta_B = 633/\Lambda$. The distance between the read beam and the diffracted signal, $D_r$, at the 'standard" distance of 24 inches is then $D_r = 2*24\sin\theta_B$. We adjust the read beam mirror on the translation stage so that the read beam hits a test screen placed 24 inches from the sample a distance $0.5(D_r - D_w)$ outside of the write beam. The diffracted signal is then found the equivalent distance on the other side. This works – a little tweaking of the mirror is then done to get the strongest signal.

Wavelength Selection.

This is straight forward. The upper portion of Fig. 6-2 shows the layout. A prism is a better choice than a grating because a grating would produce multiple orders. We "hand adjust" the prism and the aperture to get the desired wavelength. A laser with built in wavelength selection would be a better choice.

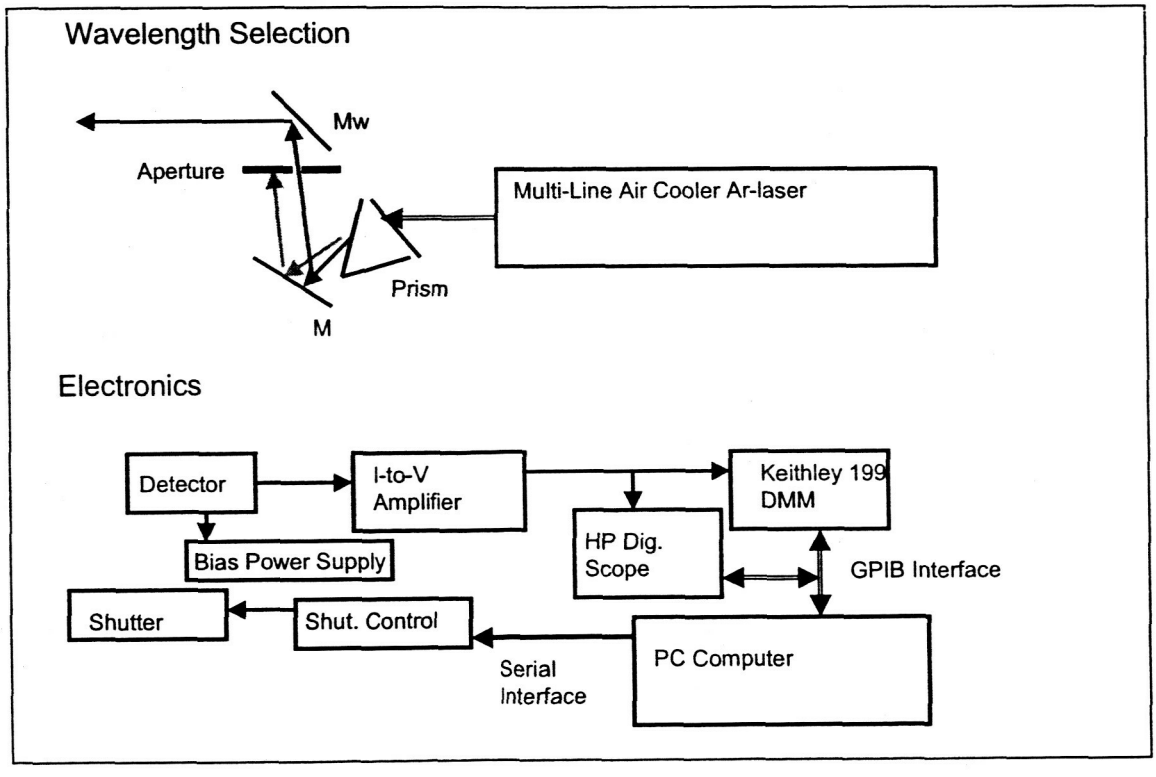


Figure 6-2. The wavelength selection layout and an electronics block diagram.

Electronics.

We have used three different types of detectors. (1) The simplest and least expensive is a Si-photodiode. These work OK but are not very sensitive. (2) Most of our data has been taken using a 931B photomultiplier tube, PMT, operated with 700 V bias. This tube was initially chosen because we salvaged it from some old equipment. We replaced it once and it may be going out again. (3) We are currently trying a Si-avalanche photodiode, Si-apd, from Advanced Photonix. It is slightly less sensitive than the PMT but appears to be satisfactory for our experiments. It also requires a bias voltage; we are using 220 V. The sensitivity depends on the bias and it may be possible to increase it. PMTs are probably the best choice. Hammamatsu is a good source. (They also sell Si-apds.) They make miniaturized units that include the bias supply –if we were starting over we would probably try one of these units. The Si-apd is a good second choice . They are not inexpensive, ours was $270. However, they are small and easily mounted. The detector needs to be positioned and aimed for the best signal. So small is good. It should be on an easily moveable mount (like a magnetic base) with vertical and horizontal translation and rotation. A HeNe laser line filter (passes only 633nm) should be installed with the detector to keep out stray light and prevent accidental damage from room light.

All of these optical detectors produce a current output and the I-to-V amplifier is used to convert the small current signal into a voltage. We use a very old Keithely 617. Stanford Research and the optics companies Newport, Oriel, etc. have commercial units. If money is really tight one can make useable units from a LM301 (a 101 would be better) operational amplifier.

The digital scope and the DMM are straight forward. The only thing that we do with them that is unusual is to operate the DMM as a data-logger. This allows it to collect the slow portion of the decays while the scope simultaneously collects the fast part of the signal. Not all DMMs have the data logging feature so some caution is needed in selecting one. I suspect that one could also do some of this with a DAQ card in the computer.

The shutter is from JMLDirect (www.jmloptical.com) and is controlled with their SDT16560 controller. The controller has a serial interface so the shutter can be fired by the computer. It can also be fired by an externally generated TTL signal.

## 7. Wetting Studies of Bismuth Silicate ($Bi_{12}SiO_{20}$) on Platinum-5%Gold

One of the fundamental issues in Bridgman growth of any material, and BSO in particular, is the interaction with the confinement material. If the confinement material and the solidified crystal have different thermal expansion coefficients, the crystal cannot contract during cooling and this leads to stresses in the crystal. These stresses can be avoided by using a non-wetting confinement material or one with similar thermal expansion properties. Unfortunately, the corrosiveness of the BSO melt does not provide many material choices, and platinum has been used exclusively for growth from the melt. Throughout the literature, it is documented that molten oxides, including BSO, will attack platinum labware [27,176-187] .It is therefore necessary to study the interaction between BSO and the confinement material.

The contact angle of Bismuth Silicate ($Bi_{12}SiO_{20}$, BSO) on platinum/5% gold was measured using the sessile drop method. Contact angles were measured from drop images. In addition, drop edge profiles were used to generate a Laplacian curve for the drop numerically in order to also obtain a surface tension value. Examination of the substrate showed that surface scratches did not affect the drop shape but that grains did. It was found that drop edge pinning occurred at the grain boundaries of the substrate. Additionally, a contact angle hysteresis was observed. The sessile drop method was found to be unsuitable for determining the contact angle and surface tension of Bismuth Silicate on platinum/5% gold because several underlying assumptions are not met and the low contact angle only provides a small portion for fitting of the Laplacian curve.

## 7-1. Sessile Drop Experiments

The sessile drop experiments are based on the finding the equilibrium state between the solid, liquid, and vapor phase interfacial tensions. Figure 7-1-1 shows a schematic of a sessile drop and the interfacial tensions. The balance of these forces if given be Young's Equation (Eq 1):

$$\cos\theta_E = \frac{\gamma_{s/v} - \gamma_{s/l}}{\gamma_{l/v}} \qquad \text{Eq 1}$$

where
$\theta_E$: equilibrium contact angle
$\gamma_{l/v}$: liquid/vapor interfacial energy ($mJ/m^2$)
$\gamma_{s/v}$: solid/vapor interfacial energy ($mJ/m^2$)
$\gamma_{s/l}$: solid/liquid interfacial energy ($mJ/m^2$)

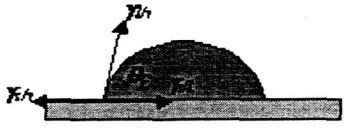

Figure 7-1: Surface tension forces in a sessile drop configuration

The balance of forces acting on the drop governs the shape of the sessile drop. Gravity tends to flatten the drop while surface forces tend to make it spherical. The Laplace equation of capillarity is this mechanical balance of forces and is given in Equation 2. It relates the pressure difference across a curved interface to the surface tension and curvature of the interface. For two homogeneous fluids that are separated by an interface, it is the mechanical equilibrium condition.

$$\gamma\left(\frac{1}{R_1} + \frac{1}{R_2}\right) = \Delta P \qquad \text{Eq. 2}$$

where
$R_1$, $R_2$ : principal radii of curvature (m)

?P: pressure difference across interface ($N/m^2$)
$\gamma$ : interfacial tension ($mJ/m^2$)

If no other forces are present, the change in pressure can be expressed as a linear function of elevation (Eq 3).

$$\Delta P = \Delta P_0 + (\Delta \rho) g z \qquad \text{Eq 3}$$

where
$?P_o$: change in pressure at a reference plane
?$\rho$: change in density
g: acceleration due to gravity
z: vertical height of drop measured from the reference plane

**Experimental**

The furnace used for sessile drop experiments is shown in Figure 2. The heating element consisted of Fe-Cr-Al windings embedded in aluminum-silica insulation (Watlow, 700W). A quartz tube was with fitted end-caps that allowed for imaging one end and control of ambient composition from the other. A bubbler with glycerin was used to ensure constant pressure within the tube that was slightly above atmospheric pressure. Copper tubing was used to cool to quartz tube in order to avoid overheating of the o-ring on the end-cap. The alumina sample holder is shown in Figure was mounted on a ceramic tube used for insertion of the sample into the center of the furnace.

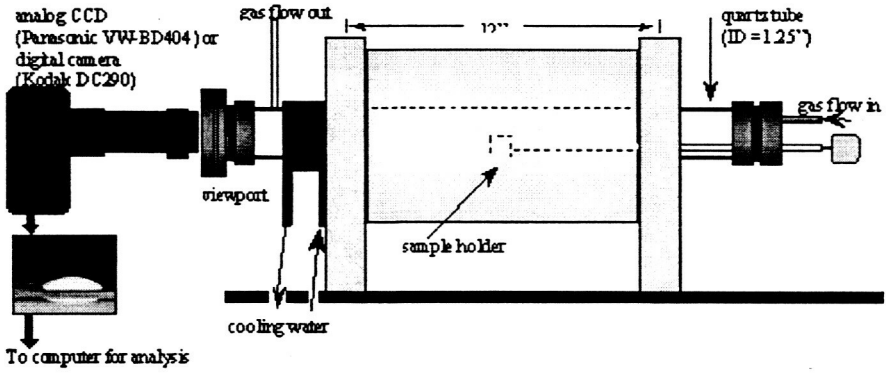


Figure 2: Experimental Setup for sessile drop experiments

Platinum-5%gold sheets were ordered with a mirror finish for use as substrate for the sessile drops. However, as delivered samples had uniform scratches. The platinum substrates were polished with colloidal silica solution (0.02-0.05 µm, pH 10) on a long nap pad (S Deman cloth, Struers). A pressure of 30 N and 50-100 rpm were used for all substrates. Surface variations were measured with a profilometor. Finally, the sheet was cleaned with DI water and heated to a 1000 °C for 30 minutes prior to the experiment

The substrate and sample were inserted into the furnace and aligned using digital images to ensure that the substrate was horizontal. The tube was purged for 10 minutes with the gas (0.1 % oxygen, balance argon). The sample was then heated to the melting

point and images of the drop were taken using either an analog CCD camera (Panasonic VW-BD404) or a digital camera (DC290, Sony).

**Results**

.Contact angles were also obtained from numerical curve fitting of the experimental data. Computational results were within error limits (one standard deviation)for almost all images. No significant difference between the contact angle of BSO on Pt-5%Au found in this work and the contact angle of BSO on pure platinum [72] found in previous work was observed.

Computed surface tension values varied drastically between experiments and within a given data set. It was suggested [193] that computational modeling using of sessile drop is inappropriate for contact angles significantly less than 90 °.This is due to the fact that too little of the Laplacian curve is available for curve fitting and related errors become too large. Uniform scratches, with an amplitude approximately +/-0.5 μm, were found on the 'as delivered ' substrate but did not affect the geometry of the drop.These scratches were on the same order as grain height variation on polished samples. Drop diameter and contact angles showed a temperature dependence and a hysteresis effect.Repeated melted and solidification of a drop on the same substrate resulted in a variation in drop diameter and contact angle. Behavior of the melt contact line was seen to be dominated by pinning at the grain boundary as shown by micrographs of the substrate and in situ images.Assumptions in the sessile drop technique that could not be satisfied in the experiments include

(a) that the surface is homogenous and smooth
(b) that no other forces besides surface tension and gravity are present.

Therefore it is concluded that the sessile drop technique is inappropriate for studying the wetting behavior of BSO melts on platinum and platinum-5%gold substrates. Although contact angle data and surface tension values could not reliably determined in this work, the discovery of grain boundary pinning is important because it helped identify the deficiencies associated with this method for the BSO-platinum and BSO-platinum/5%gold systems. Future wetting work on any system with a polished metal surfaces will need to analyze the effect of grain boundaries to ensure that assumptions made in modeling a sessile drop are met.

**7-2.Reduced Gravity Wetting Experiments:KC-135**

Witt et al.194 reported that in microgravity some systems exhibit a different wetting behavior than on the ground.

Early proposed designs for ampoule configurations were aimed at minimizing contact between the melt and the confinement material in an effort to establish a free solid-liquid interface. Such designs would have allowed for interface demarcation using current pulses. However, these designs depended on certain wetting behavior between the melt and the confinement material. In order to investigate the effect of gravity on the wetting behavior of

BSO on platinum and platinum/5%gold,reduced gravity wetting experiments were conducted in the KC-135.The scope of the KC-135 experiments was a phenomenological comparison of the melting and re-solidification behavior of BSO in a reduced gravity (10 -2 g)environment versus on in a terrestrial (one g)environment.
The reduced gravity environment was achieved by flying the KC-135 airplane along a parabolic trajectory (Figure 7-2-1).

At the top of the parabola, approximately 20 seconds of reduced gravity
(on the order of 10 -2 g) were experienced by all objects and persons inside the aircraft.
Each flight typically consists of forty such parabolas.

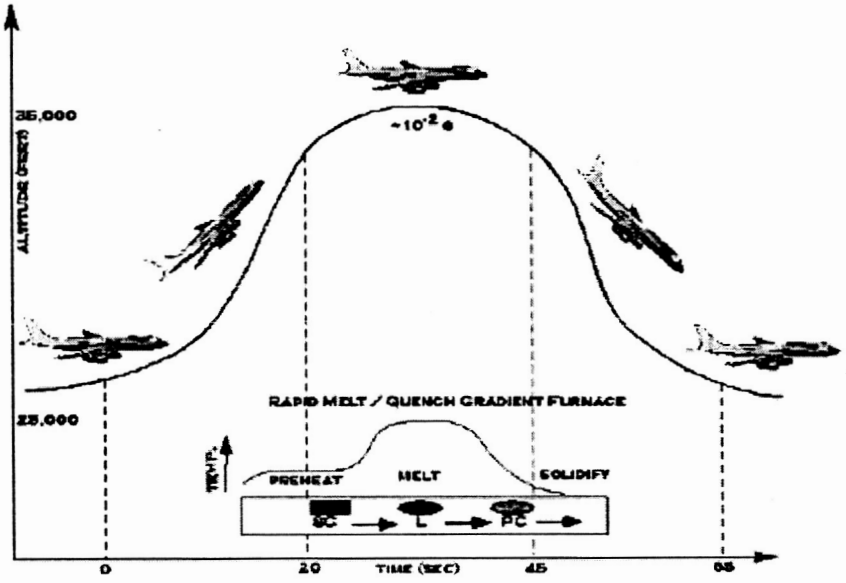


Figure 7-2-1 A schematic representation of the flight path.

## Experimental Procedure

The ampoule was loaded once the plane had taken off. The furnace was then ramped to the correct setpoints. Samples were heated to 850 °C in the preheat zone. As the plane entered the low gravity period of the chosen parabola,the ampoule was translated into the rapid melt zone for 15 seconds and quenched with a helium quench after rapid translation out of the heater. The temperature profile is shown in Figure 4-18(b).Ampoules could not be removed from the furnace until the plane was flying level,and this occurred every 8-10 parabolas for about 5 minutes. During this time, the processed ampoule was removed and a new ampoule was loaded.

## Results

Samples that were processed successfully melted partially and solidified before the low gravity period ended. A number of samples were not quenched properly due to hardware deficiencies. Although no quantitative contact angle measurements can be made,there is no qualitative difference in the fundamental wetting behavior in low gravity as compared to terrestrial conditions. The acceleration environment for the sample is shown in Figure 7-2.

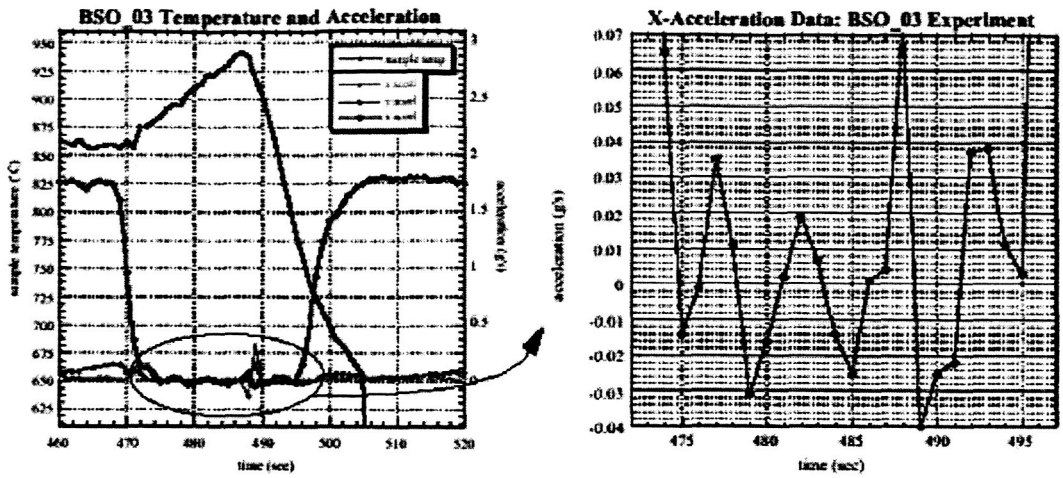


Figure 7-2. The data for sample #3 showing residual and vibrationally induced accelerations.

The spike present 15 seconds into the low gravity period is due to the motion of the furnace from the hot zone to the quench zone. Due to residual acceleration,molten material flowed to one or the other end where it solidified.As an example,top and bottom views of sample #3 after processing are depicted in Figure 7-3.

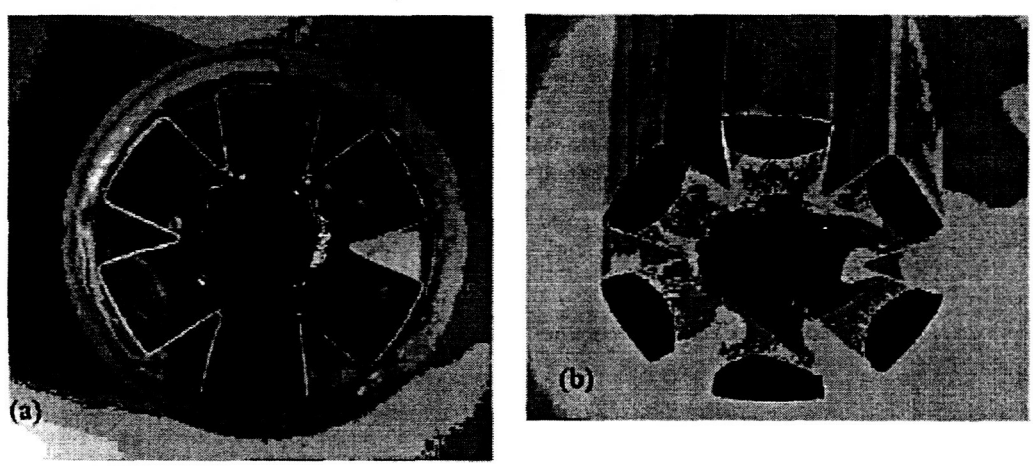


Figure 7-3. Procesed KC-135, sample #3, (a) top view, (b) bottom view.

The bottom view (b)clearly shows how the melt solidified in contact with the Pt/Au.Most of the samples did not stay vertical in the confinement material.Thermal asymmetry in the furnace caused melting to occur on one side first, causing the sample to tilt slightly.Once contact was lost with the Pt fin, the conduction heat path was lost, and the sample did not have enough time to melt on that side as a consequence of the reduction in heat flux (see Figure 7-4.

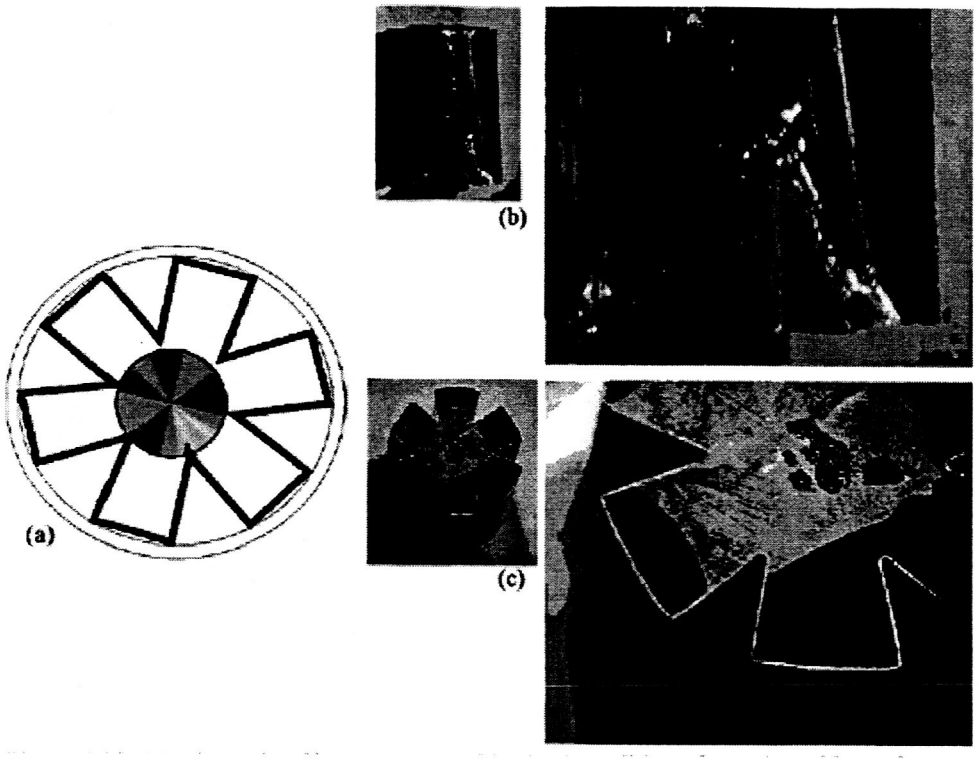


Figure 7-4. (a) schematic of how uneven melting leads to tilting of sample and loses of conduction heat transfer at some of the film tip, (b) side view of sample #5 and close-up showing no adhesion, (c) bottom view of sample #5 and close-up.

The need for thermal symmetry is therefore critical for processing in a partially confined manner and suggests the use of heat pipes in the furnace in order to achieve radial uniformity of the thermal environment. It is also clearly seen that there is no adhesion between the BSO and Pt as seen by the smooth surface of the BSO in Figure 7-4(b).

# 8. Comparative Analysis of Electro-Optic Properties in Bismuth Silicate Grown bythe Czochralski, Bridgman-Stockbarger, and Hydrothermal Techniques

## Experimental Approach

Crystals grown by three different growth techniques, Czochralski (CZ), Bridgman-Stockbarger (Bridgman or B-S), and hydrothermal, were analyzed for their optical and photo-electric properties. Czochralski crystals are grown from the melt; the unstable thermal configuration and the rotation of the crystal lead to convective interference which adversely affects crystal quality. Bridgman-Stockbarger growth is also from the melt but uses directional solidification and a stable thermal configuration to reduce convection. Hydrothermal growth is unique because growth occurs at low temperatures and high pressures using an aqueous solution.

Samples from crystals grown by the three different methods were analyzed in an effort to correlate fluctuations in energy levels and trap densities to changes in growth conditions. The growth of the Czochralski and Bridgman-Stockbarger crystals is described

elsewhere[11,12]. The hydrothermal material was obtained from crystals grown at the Air Force Research Laboratory (Hanscom Air Force Base, MA).
Absorption and photoconductivity measurements were performed. Subsequently, the photochromic response of the crystals was chosen for a more careful analysis of the effect of growth conditions on long lifetime traps. Lastly, the photorefractive response of both un-annealed and annealed samples was studied.

## Results and Analysis

### Absorption Measurements

Optical transmission measurements were used to determine the free carrier absorption near the band edge. Measurements were made at room temperature using a Cary 500 Spectrophotometer in the range from 400 to 900 nm (1.4 - 3.2 eV). Samples were prepared by mechanochemically polishing both sides. Sample thickness varied from 1.5 to 3 mm. Absorption was calculated from the transmission spectrum, sample thickness, and reflectance. Typical spectrums of two samples (BS113001 and BS020802) are shown in figure 8-1.

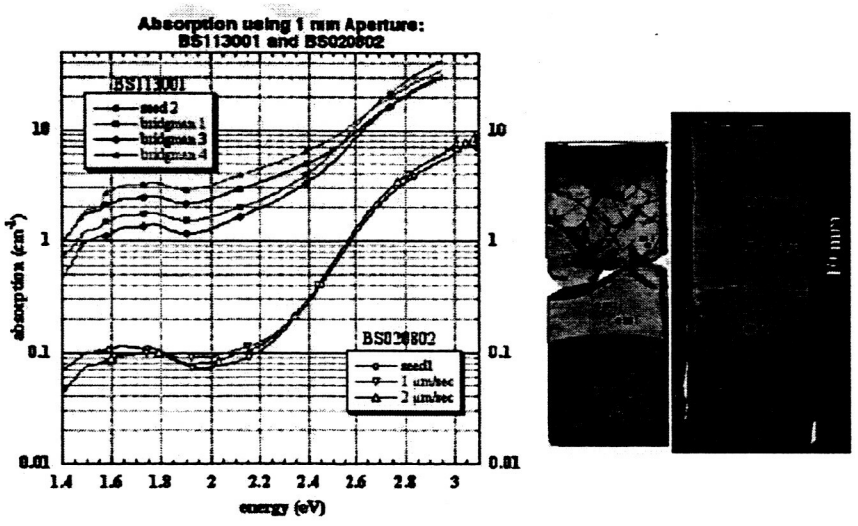


Fig.8-1.Absorption spectra for sample BS113001 and BS020802. Approximate measurement points shown on the right.

Approximate measurement points are indicated in the adjacent images. It was observed that for samples of the same thickness, material appearing darker in color exhibited a higher overall absorption, indicating a higher defect concentration.

### Photoconductivity

Samples for photoconductivity measurements were cut to approximately 5 mm x 5 mm x 3 mm. Both the illuminated and back side and all the edges were polished using Syton solution on a Chemomet I (Buehler) polishing pad. Electrical contacts were made on the edges using a silver paste. Prior to taking photoconductivity measurements, samples were

annealed in darkness at approximately 150 °C. During the measurements, samples remained in the dark, and the current that passed through the sample was kept constant. Samples were illuminated at low intensities by a Perkin-Elmer monochromater. Measurements were made at 77 K in the spectral range from 0.2 to 2.4 eV. Results from photoconductivity measurements from the three types of crystals are shown in Figure 8-2.

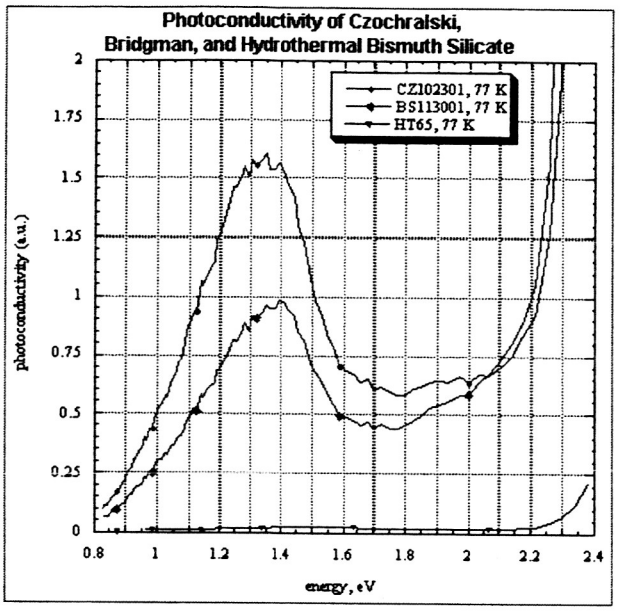


8-2. Photoconductive response for Czochralski, Bridgman, and Hydrothermal material.

Both the Czochralski and the Bridgman material exhibited a single peak near 1.35 eV. The hydrothermal material did not exhibit a peak at this energy level, indicating the absence of the defect responsible for the trap at that level. Unfortunately, the absolute magnitude of the photoconductivity signal from the different samples (i.e. CZ vs. B-S vs. hydrothermal) could not be directly compared in these measurements because the current used to generate the voltage difference across the electrodes differed for each sample. This was necessary in order to maximize signal to noise ratio. However, the current setting for the B-S sample was approximately 10 times smaller than the setting for the CZ sample. This signified an increased resistivity due to a decreased trap density in the Bridgman type material. Since conductivity is proportional to carrier density, it can be concluded that the defect concentration was lower in the Bridgman material and lowest in the hydrothermal material as compared to the Czochralski material.

The photoconductivity spectrum of BSO changed when samples were exposed to background illumination (visible, UV light) prior to taking measurements. The illumination caused electrons to be transferred from shallow acceptors to traps via the conduction band. As a result of this transfer, the acceptors and traps both became deeper levels and were charged. The material was therefore excited at energies that differed from the dark conductivity spectrum. A typical photoconductivity spectrum of illuminated BSO is shown in Figure 8-3.

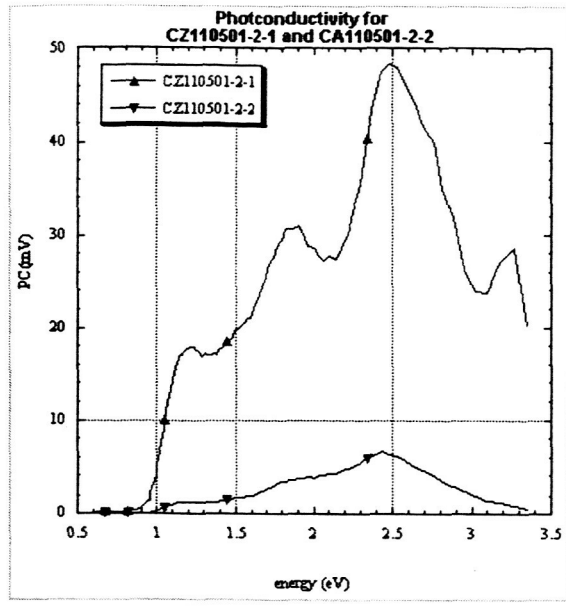


Figure 8-3. A typical photoconductivity spectrum of illuminated BSO.

**Photochromic Response Measurements**

The photochromic effect occurs when carriers are excited into the conduction band, and the localized ground state transforms into a metastable de-localized excited state that is accompanied by a lattice relaxation[13]. A change in the absorption spectrum results from this process. A number of samples representing the different conditions were cut from two Czochralski boules (identified as CZ102301 and CZ110501) and two Bridgman-Stockbarger crystals (labeled BS1130001 and BS020802) and polished as described in the absorption section above. Photochromic response was measured by comparing absorption spectra before and after illumination. Samples were dark annealed at elevated temperatures (200-300 °C) to thermally empty traps. Identical sample holders with a two millimeter aperture were manufactured for absorption measurements. Samples were mounted on the holders prior to the dark anneal. Samples could then reliably be loaded into the spectrophotometer with minimum exposure to the 'red' light present while inserting the samples. A 'dark' absorption spectrum (400-900 nm) was taken; the sample was then exposed to 'white' light for one minute using a halogen lamp. Next, an illuminated absorption spectrum (400-900 nm) was acquired from the same sample. The change in the absorption behavior due to exposure to the optical stimulation was assessed by analyzing the ratio of the illuminated spectrum to the dark spectrum as is shown in Figure 4(a)and (b).

It was observed that the 'dark' spectra of the Bridgman samples were different than those from the Czochralski samples. In the CZ samples it appeared that several traps were emptied due to the dark anneal as is indicated by the fact that their 'dark' spectra did not have any peaks. The dark anneal did not have as marked an effect in the B-S samples. Moreover, the seed (data marked BS113001-S) that was cut from the CZ102301 boule exhibited a reduced photochromic response when compared to samples from the same area of that boule that had not been used as seed material.

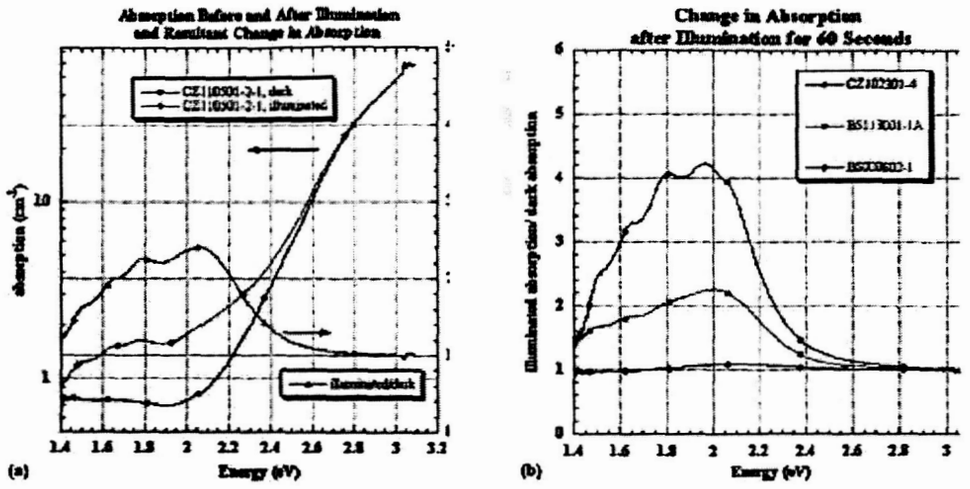


Fig.4. (a)Dark and illuminated spectra and resulting ration,(b)ratios for several different samples (CZ- Czochralski, B –S Bridgman –Stockbarger).

Figure 7-4(b) shows the ratio of illuminated to dark absorption from one of the CZ samples and two of the Bridgman samples. Looking at the ratio of illuminated to dark absorption, there are five discernible peaks in the CZ data. This indicates that the photochromic effect is not due to a single trap, but rather, that several energy levels are involved. These peaks are not present in the BS113001 data. However, most unique is the fact that one of the Bridgman crystals, BS020802, did not exhibit any photochromic response at all.

**High Temperature Annealing Effects**

The effect of high temperature annealing (near melting point – about 865 °C) was discovered as a result of the photochromic response measurements. The first indication was the absence of any photochromic response in samples that came from the Bridgman crystal that was grown in a low thermal gradient (BS020802). Not only was there no difference between the dark and illuminated spectra for the regrown material, more importantly, it was found that the seed material did not show any change either. Since samples from the Czochralski boule from which that seed was cut showed photochromic behavior, it was concluded that the seed material was modified during Bridgman growth process. Looking at the temperature data, it was noted that the seed was exposed to temperatures near the melting point for over 12 hours. It was hypothesized that the defect concentration was permanently altered as a result of this high temperature anneal.

In order to test this theory, Czochralski material was sealed in an ampoule and annealed using the same thermal profile that was experienced by the seed of BS020802. The photochromic response was almost completely removed in that CZ sample (data labeled 'CZ102301-high T annealed'). Figure 7-5 shows the ratio of illuminated to dark spectra from several samples that were annealed at high temperatures on an expanded scale. The maximum lies in the vicinity of 585 nm (2.1 eV). For annealed samples, it was the spectra that was taken prior to illumination (the 'dark' spectra) that was different than in unannealed samples. The thermal anneal at 275 °C in the dark no longer emptied the traps, i.e. the dark spectra were the same as the illuminated spectra rather than vice versa. It was also found that the photochromic response was only removed if the high temperature anneal occurred in a sealed ampoule.

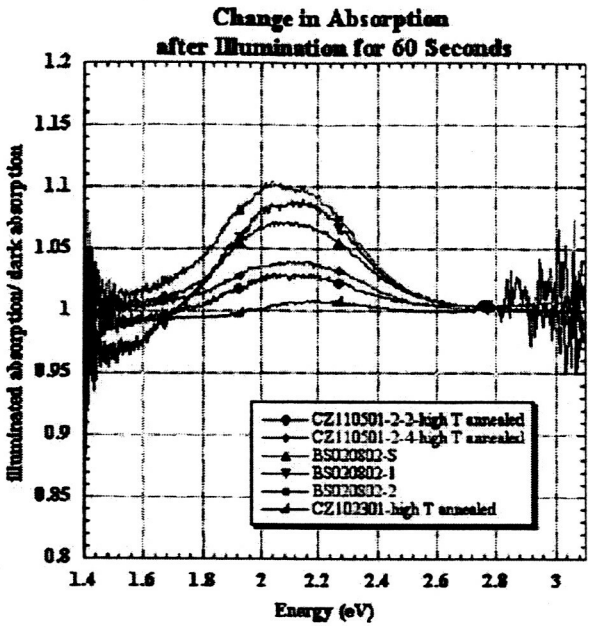


Fig.7-5.Photochromic response of samples annealed at high temperatures.

It is documented in literature that annealing chromium doped BSO[14] and Mn-doped BTO[15] in a vacuum removes the photochromic effect, but that this process can be reversed by annealing the samples in air. A sample that had been annealed at high temperatures and exhibited no photochromism was re-annealed in air. The photochromic response was restored in the sample. Therefore, it was concluded that oxygen vacancies were formed during annealing in a reduced oxygen environment and that this had a fundamental effect on the interband states. Panchenko[14] also concluded that the number of oxygen vacancies was increased with vacuum annealing, and that as a result, the number of oxygen atoms available for ionization for light induced transitions decreased.

To further investigate the modification of the interband states, photoconductivity measurements of unannealed and annealed samples were taken. For these measurements, the geometrical configuration of the electrodes was changed from the earlier measurements. The resistance decreased width sample thickness. This resulted in a better signal to noise ratio and allowed for higher spectral resolution. Additionally, the new configuration allowed for the same current setting to be used for all samples. Direct comparison of signal strengths between samples was thus possible. The response in the annealed sample was approximately six times weaker than that of the unannealed sample, as seen in Figure 7-6.

The resistance did not significantly vary between these samples indicating that the carrier concentration was about the same. Therefore, the decrease in signal strength was concluded to be due to a decrease in carrier lifetime.

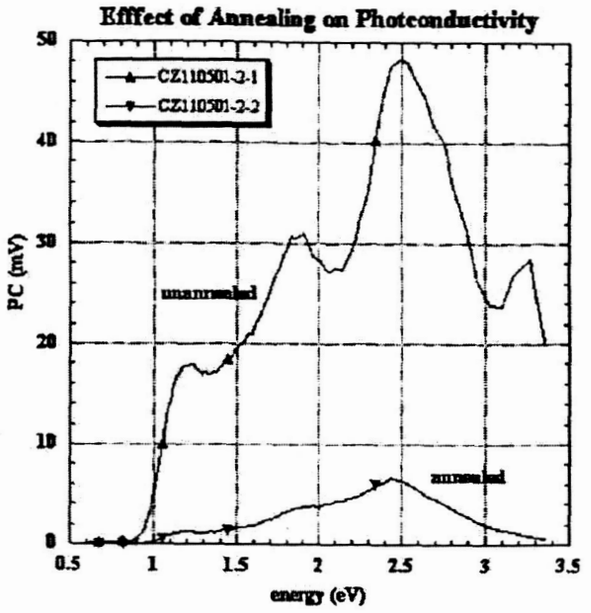


Fig.7-6. Effect of annealing on photoconductivity.

**Photorefractive Response**

Photorefractivity measurements were performed on annealed and unannealed samples. A four beam mixing set-up was used at Oklahoma State University in collaboration with Prof. Martin. An argon laser (488 nm, 15 mW setting) was used for the write beams. The beams were crossed such that a two micron grating was created. A HeNe laser (633 nm) was used for the read beam. The set-up is described in detail elsewhere[16]. Gratings were written for 0.5 seconds and the subsequent decay was monitored for 20 seconds. The diffracted read beam signal was measured with a photo multiplier tube, amplified, sent to an high precision digital voltmeter and an oscilloscope, and both signals were logged to a data file. The oscilloscope recorded the first second (including the write cycle) with a resolution of one millisecond. The higher resolution DVM recorded for 20 seconds but only at 100 ms intervals. Samples were dark-annealed at 250 °C overnight to thermally empty traps prior to data acquisition.

The annealed samples showed a fundamentally different photorefractive response than the unannealed samples as well as any photorefractive response published by others.

The signal was weaker, had a different rise time, and exhibited a different decay behavior. The signal strength for annealed samples was reduced by a factor of approximately six as compared to unannealed samples of comparable thickness. A comparison of the two signal strengths is shown in Figure 7-7.

The leading edge peak was narrower in annealed samples than in unannealed samples. Figure 7-8 shows the scans from Figure 7-7 but with the leading peak of the annealed sample scaled to the same height as the leading peak of the unannealed sample and translated such that the maximums coincide.

It is concluded that the response time had decreased due to the modification of the interband states during the high temperature anneal.

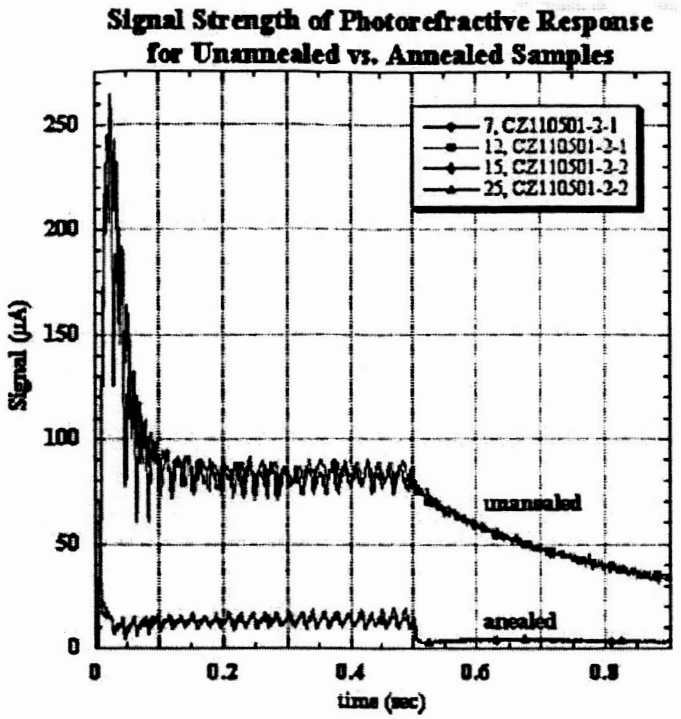


Fig.7-7.Strength of photorefractive response for unannealed and an-nealed samples.

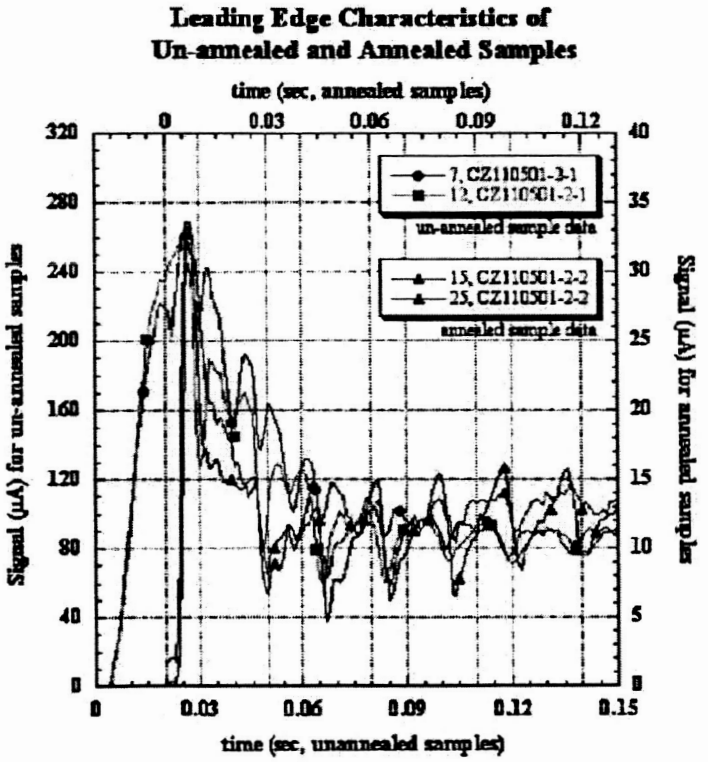


Figure 7-8. The leading edge peak in annealed and in unannealed samples.

The decay of the read beam was substantially different in the annealed samples as compared to the unannealed samples.

The decay of the unannealed sample was characteristic of the response for BSO as observed and published by Prof. Martin in his research. Figure 7-9 shows the differences in decay behavior for annealed vs. unannealed samples.

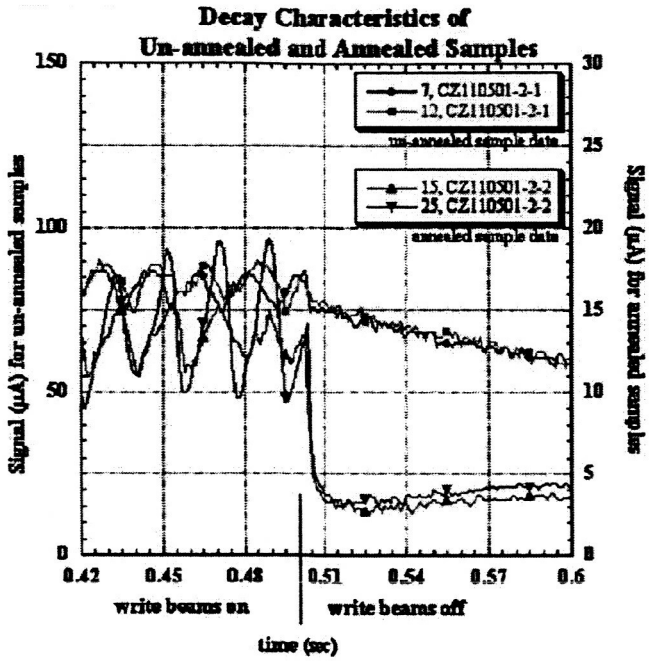


Figure 7-.9.Difference in initial decay for unannealed and annealed samples after write beams are turned o .(scope data).Annealed signal is scaled 5 x.

The annealed samples exhibited decay in multi-step fashion. There was an initial, very fast, decay that was then followed by a very slow decay. Figure 10 is a plot of the read beam strength after the read beam has been turned off.

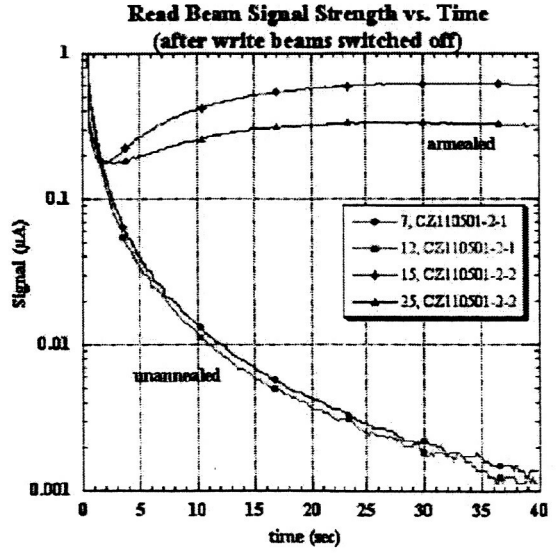


Figure 7-10.Difference in long decay for unannealed and annealed samples after write beams are turned off.

The signals have been normalized with the read beam signal strength just prior to the write beams being turned off so that the decay characteristics can be compared independent of the magnitude of the signal.
Photoconductivity determines the speed of photorefractive build-up as well as the decay of $\Delta n$[17]. Examining the photorefractivity data, this is clearly evident. The leading peak as well as the initial decay in the annealed samples are faster than in the unannealed case as seen in Figure 8 and Figure 9. The data supports the conclusion that the time constant for these processes is smaller in the annealed samples than in the unannealed samples.
The best explanation for the unusual decay behavior of the annealed samples is that trap levels were modified during the high temperature anneal and that carriers decay back to the ground state through a different pathway than in unannealed samples. However, the complexity of the structure of impurity levels and traps in BSO made a detailed analysis beyond the scope of current work and will be the subject of future research.

## Conclusions

A comparative analysis of electro-optic properties of Czochralski, Bridgman-Stockbarger, and hydrothermal material was performed in order to investigate the origin of the critical native defect. The results clearly indicate that the growth and processing conditions of BSO can fundamentally affect the electro-optic properties of the material.
The analysis indicated that Czochralski material contained the highest density of both native defects and residual impurities. This is indicated by the largest photoconductivity signal and strongest photochromic response. However, the distribution of defects is highly nonuniform and to a large extend uncontrollable in CZ material[11].
Absorption, photoconductivity, and photochromic response indicated a lower defect concentration in Bridgman-Stockbarger material as compared to Czochralski material. However, the distribution of defects in B-S material is more uniform[12] than in Czochralski material due less convection during growth. The hydrothermal material did not contain the critical native defect and hence did not exhibit photoconductivity or photorefractivity.
The atmosphere during growth and annealing was found to be a crucial factor in the creation the electro-optically active defects. Room temperature photochromism was absent in the only Bridgman sample that was processed in a sealed environment. Subsequent experiments showed that the photochromic response could be removed by high temperature annealing, but that it had to occur in a sealed ampoule. Additionally, the photochromic effect could be re-established by annealing in air. These observations led to the conclusion that the availability of oxygen atoms in the atmosphere during growth and processing is necessary in order to keep the $Bi_2O_3$ - $SiO_2$ system in equilibrium. If there is a deficiency of oxygen in the processing environment, oxygen vacancies will be created and affect the electro-optic properties as a result.
Photoconductivity in annealed samples was a factor of six lower than in unannealed samples. Photorefractivity was also substantially altered due to the high temperature anneal. The leading edge peak as well as the initial grating decay in annealed samples indicated a faster dynamic response. The changes in photoconductivity and photorefractivity in annealed samples lead to the conclusion that high temperature annealing decreased the lifetime of some of the traps. However, long time decay of the photorefractive signal slowed drastically. Persistent gratings were left in annealed material that could only be erased with 488 nm uniform exposure. Comparison of decay curves for annealed and unannealed

samples indicated that several traps must be involved in the decay process. However, the exact mechanism for modification of defect interaction could not be unambiguously identified from current data.

This work showed that the electro-optic properties of BSO are highly dependent on the growth conditions including the thermal environment, the growth technique used, and the ambient atmosphere. Additionally, post growth processing can also significantly affect the material's response. For this reason, in order to perform valuable analysis of sillenite electro-optic properties, growth conditions must be quantitatively known, controllable, and reproducible.

## References


1. Ashkin, A., G. D. Boyd, et al. (1966). Appl. Phys. Letters 9 (1), 72-4.
2. Fainman, Y., J. Ma, et al. (1993). Materials Science Reports 9 (2-3), 53-139.
3. Huignard, J. and F. Micheron (1976). Applied Physics Letters 29 (9), 591-593.
4. Peltier, M. and F. Micheron (1977). Journal of Applied Physics 48 (9), 3683-3690.
5. Yeh, P. (1987). Applied Optics 26 (16), 3190-3191.
6. Jones, A. D. W. (1983). Journal of Crystal Growth 61, 235-244.
7. Witt, A. F. (1991). "Identification and Control of Gravity Related Defect Formation during Melt Growth of Electro-optic Single Crystals: Sillenites (Bi12SiO20)". NASA proposal.
8. Ballman, A. (1967). Journal of Crystal Growth 1, 37-40.
9. Oberschmid, R. (1985). Phys Stat Sol (A) 89, 263-270.
10. Larkin, J., M. Harris, et al. (1993). Journal of Crystal Growth 128, 871-875.
11. Wiegel, M.E.K. (2003). "Growth and Defect Analysis of Czochralski Grown Bismuth Silicate ($Bi_{12}SiO_{20}$)" submitted for publication to Journal of Crystal Growth.
12. Wiegel, M.E.K. (2003). "Investigation of the Relationship between Growth Conditions and Defect Incorporation in Bismuth Silicate ($Bi_{12}SiO_{20}$) Grown in a Vertical Bridgman-Stockbarger Furnace" submitted for publication to Journal of Crystal Growth.
13. Becla, P. (2002). private communications.
14. Panchenko, T. V. and N. A. Truseyeva (1991). Ferroelectrics 115 (1-3), 73-80.
15. Volkov, V. V., A. V. Egorysheva, et al. (1993). Inorganic Materials 29 (11), 1364-1374.
16. McCullough, J. S., A. L. Harmon Bauer, et al. (2001). Journal of Applied Physics 90 (12), 6022-6025.
17. Vogt, H., K. Buse, et al. (2001). Journal of Applied Physics 90 (7), 3167-3173.

uniform exposure. Comparison of decay curves for annealed and unannealed samples indicated that several traps must be involved in the decay process. However, the exact mechanism for modification of defect interaction could not be unambiguously identified from current data.

This work showed that the electro-optic properties of BSO are highly dependent on the growth conditions including the thermal environment, the growth technique used, and the ambient atmosphere. Additionally, post growth processing can also significantly affect the material's response. For this reason, in order to perform valuable analysis of sillenite electro-optic properties, growth conditions must be quantitatively known, controllable, and reproducible.

**References**


1. Ashkin, A., G. D. Boyd, et al. (1966). Appl. Phys. Letters 9 (1), 72-4.
2. Fainman, Y., J. Ma, et al. (1993). Materials Science Reports 9 (2-3), 53-139.
3. Huignard, J. and F. Micheron (1976). Applied Physics Letters 29 (9), 591-593.
4. Peltier, M. and F. Micheron (1977). Journal of Applied Physics 48 (9), 3683-3690.
5. Yeh, P. (1987). Applied Optics 26 (16), 3190-3191.
6. Jones, A. D. W. (1983). Journal of Crystal Growth 61, 235-244.
7. Witt, A. F. (1991). "Identification and Control of Gravity Related Defect Formation during Melt Growth of Electro-optic Single Crystals: Sillenites (Bi12SiO20)". NASA proposal.
8. Ballman, A. (1967). Journal of Crystal Growth 1, 37-40.
9. Oberschmid, R. (1985). Phys Stat Sol (A) 89, 263-270.
10. Larkin, J., M. Harris, et al. (1993). Journal of Crystal Growth 128, 871-875.
11. Wiegel, M.E.K. (2003). "Growth and Defect Analysis of Czochralski Grown Bismuth Silicate ($Bi_{12}SiO_{20}$)" submitted for publication to Journal of Crystal Growth.
12. Wiegel, M.E.K. (2003). "Investigation of the Relationship between Growth Conditions and Defect Incorporation in Bismuth Silicate ($Bi_{12}SiO_{20}$) Grown in a Vertical Bridgman-Stockbarger Furnace" submitted for publication to Journal of Crystal Growth.
13. Becla, P. (2002). private communications.
14. Panchenko, T. V. and N. A. Truseyeva (1991). Ferroelectrics 115 (1-3), 73-80.
15. Volkov, V. V., A. V. Egorysheva, et al. (1993). Inorganic Materials 29 (11), 1364-1374.
16. McCullough, J. S., A. L. Harmon Bauer, et al. (2001). Journal of Applied Physics 90 (12), 6022-6025.
17. Vogt, H., K. Buse, et al. (2001). Journal of Applied Physics 90 (7), 3167-3173.
17.


## List of publications, presentations and posters in support of this Project

**Publications:**

Wiegel M.E.K, Becla P., "Comparative Analysis of Electro-Optic Properties in Bismuth Silicate Grown by the Czochralski, Bridgman-Stockbarger, and Hydrothermal Techniques" Optical Materials, Article in press, 2004, Alsevier B.V.

Wiegel, M.E.K. "Czochralski Growth and Defect Analysis of Bismuth Silicate (Bi12SiO20)." *in preparation* for submission to Journal of Crystal Growth.

Wiegel, M.E.K. "Investigation of the Relationship Between Growth Conditions and Defect

Incorporation in Bismuth Silicate (Bi12SiO20) Grown in a Vertical Bridgman-Stockbarger Furnace." *in preparation* for submission to Journal of Crystal Growth.

Wiegel, M.E.K. and August F. Witt "Wetting behavior of Bismuth Silicate on Platinum/5%Gold in terrestrial and low-gravity " *in preparation* for submission to Journal of Crystal Growth

**Presentations:**

Wiegel, M.E.K and August F. Witt. "Investigation of the Relationship Between Growth Conditions and Defect Incorporation in Bismuth Silicate (Bi12SiO20) Grown in a Vertical Bridgman-Stockbarger Furnace." Presented at the 15th American Conference on Crystal Growth and Epitaxy in Keystone, CO (July 2003).

Wiegel M.E.K, Becla P., Martin J.J., and August F. Witt. "Comparative Analysis of Electro-Optic Properties in Bismuth Silicate Grown by the Czochralski, Bridgman-Stockbarger, and Hydrothermal Techniques" Presented at the 15th American Conference on Crystal Growth and Epitaxy in Keystone, CO (July 2003).

Wiegel, M.E.K. and August F. Witt. "Vertical Bridgman Stockbarger Growth of BSO (Bi12SiO20): Melt stability and defect formation in a ground-based environment ". Presented at the 13th American Conference on Crystal Growth and Epitaxy in Burlington, VT (August 2001).

**Posters:**

Wiegel, M.E.K and August F. Witt. "Czochralski Growth and Defect Analysis of Bismuth Silicate (Bi12SiO20)." Presented at the 15th American Conference on Crystal Growth and Epitaxy in Keystone, CO (July 2003).

Wiegel, M.E.K. and August F. Witt. "Design Issues of Microgravity Oxide Single Crystal Growth Experiments: Bismuth Silicate (Bi12SiO20)". Presented at the 1st International Conference on Microgravity in Sorrento, Italy (September 2000)

Wiegel, M.E.K. and August F. Witt. "Wetting Behavior and Interaction of Bismuth Silicate (Bi12SiO20) on Platinum/5% Gold Substrates". Presented at the 12th American Conference on Crystal Growth and Epitaxy in Vail, CO (August 2000).